



1           **Long-term monitoring of atmospheric TGM at a remote high**  
2           **altitude site (Nam Co, 4730 m a.s.l.) in the inland Tibetan Plateau**

3    Xiufeng Yin <sup>1,2,3,4</sup>, Shichang Kang <sup>1,5</sup>, Benjamin de Foy <sup>4</sup>, Yaoming Ma <sup>2,5</sup>, Yindong Tong <sup>6</sup>, Wei Zhang  
4    <sup>7</sup>, Xuejun Wang <sup>8</sup>, Guoshuai Zhang <sup>2</sup>, Qianggong Zhang <sup>2,5</sup>

5    <sup>1</sup>State Key Laboratory of Cryospheric Science, Northwest Institute of Eco-Environment and Resources, Chinese Academy of  
6    Science, Lanzhou, 730000, China

7    <sup>2</sup>Key Laboratory of Tibetan Environment Changes and Land Surface Processes, Institute of Tibetan Plateau Research, Chinese  
8    Academy of Sciences, Beijing, 100101, China

9    <sup>3</sup>University of Chinese Academy of Sciences, Beijing, 100039, China

10   <sup>4</sup>Department of Earth and Atmospheric Sciences, Saint Louis University, St. Louis, MO, 63108, USA

11   <sup>5</sup>CAS Center for Excellence in Tibetan Plateau Earth Sciences, Beijing, 100085, China

12   <sup>6</sup>School of Environmental Science and Engineering, Tianjin University, Tianjin, 300072, China

13   <sup>7</sup>School of Environment and Natural Resources, Renmin University of China, Beijing, 100872, China

14   <sup>8</sup>College of Urban and Environmental Sciences, Peking University, Beijing, 100871, China

15

16

17

18

19   *Correspondence to:* Qianggong Zhang ([qianggong.zhang@itpcas.ac.cn](mailto:qianggong.zhang@itpcas.ac.cn)) and Shichang Kang ([shichang.kang@lzb.ac.cn](mailto:shichang.kang@lzb.ac.cn))

20

21

22

23



24        **Abstract**

25        Total gaseous mercury (TGM) concentrations were continuously measured at the Nam Co Station, a remote high altitude  
26 site (4730 m a.s.l.), in the inland Tibetan Plateau, China from January 2012 to October 2014 using a Tekran 2537B instrument.  
27 The mean concentration of TGM during the entire monitoring period was  $1.33 \pm 0.24 \text{ ng m}^{-3}$  (mean  $\pm$  standard deviation (SD)),  
28 ranking the lowest value among all continuous TGM measurements reported all over China, and was lower than most of sites  
29 in the Northern Hemisphere. This indicated the pristine atmospheric environment in the inland Tibetan Plateau. Long-term  
30 TGM at the Nam Co Station exhibited a slight decreasing trend especially for summer seasons. The seasonal variation of TGM  
31 was characterized by high levels during warm seasons and low levels during cold seasons. Diurnal variations of TGM exhibited  
32 uniform patterns in different seasons: the daily maximum was reached in the morning (around 2-4 hours after sunrise), followed  
33 by a decrease until sunset and a subsequent build-up at night, especially in the summer and the spring. Regional surface re-  
34 emission and vertical mixing were two major contributors to the temporal variations of TGM while long-range transported  
35 atmospheric mercury promoted elevated TGM during warm seasons. Results of multiple linear regression (MLR) revealed that  
36 humidity and temperature were the principal covariates of TGM. Potential source contribution function (PSCF) and FLEXible  
37 PARTicle dispersion model (WRF-FLEXPART) results indicated that the likely high potential source regions of TGM to the  
38 Nam Co are central and eastern Indo-Gangetic Plain (IGP) during the measurement period with high biomass burning and  
39 anthropogenic emissions. The seasonality of TGM at Nam Co was in phase with the Indian Monsoon Index, implying Indian  
40 Summer Monsoon as an important driver for transboundary transport of air pollution into the inland Tibetan Plateau. Our  
41 results provided atmospheric mercury baseline in the remote inland Tibetan Plateau and serve as new constraint for assessment  
42 of Asian mercury emission and pollution.

43

44

45

46

47

48

49 **1 Introduction**

50 Mercury (Hg) is one of the most toxic environmental pollutant because of the easy uptake of its organic forms by biota  
51 and the neurological and cardiovascular damage to humans resulting from bioaccumulation (Schroeder and Munthe, 1998).  
52 The majority of the mercury released to the environment is emitted into the atmosphere and can be transported from emission  
53 sources to deposition sites around the globe. Unlike other metals in the atmosphere, the majority of atmospheric mercury  
54 largely exists in the elemental form (Gaseous Elemental Mercury, GEM). The global residence time of GEM is in the range of  
55 0.5-2 years due to its high volatility, low solubility and chemical stability (Schroeder and Munthe, 1998; Shia et al., 1999)  
56 allowing it to be transported over long distances (tens of thousands of kilometers) far from pollution sources. GEM accounts  
57 for more than 95% of TGM (TGM, Total Gaseous Mercury. RGM, Reactive Gaseous Mercury. TGM= GEM + RGM). RGM  
58 and Hg-P (particle-bound mercury) compounds make up the remaining fraction of mercury in the atmosphere, and these two  
59 compounds have an estimated lifetime ranging from several days to a few weeks. RGM can be expected to be removed near a  
60 few tens to a few hundreds of kilometers from their source while Hg-P is likely to be deposited at intermediate distances of  
61 hundreds to thousands of kilometers (Schroeder and Munthe, 1998).

62 East Asia and South Asia are two of the areas in the world with the fastest economic growth and the highest population  
63 density. These two areas are known for their heavily polluted air (Nair et al., 2007; Mukherjee et al., 2009) and anthropogenic  
64 mercury emissions in these areas are among the world's highest (Pirrone et al., 2010). China is the largest anthropogenic  
65 emitter of mercury worldwide with most of the emissions originating from coal combustion and non-ferrous smelting  
66 production (AMAP/UNEP, 2013; Pacyna et al., 2008). Geographically, most of China's mercury emissions are located in  
67 eastern and central China (Streets et al., 2005; Wu et al., 2016). For example, atmospheric mercury concentrations in Guizhou,  
68 one of the most important mercury producing and coal producing regions in China, was reported to be 6.2 - 9.7 ng m<sup>-3</sup> of TGM  
69 in the capital city of Guiyang (Feng et al., 2004; Liu et al., 2011; Fu et al., 2011). Industrial emission and domestic coal  
70 combustion was estimated to be the main source of TGM in Guiyang (Feng et al., 2004; Fu et al., 2011). Metropolises like  
71 Beijing, Guangzhou, Wuhan, Changchun also experienced high concentrations of atmospheric mercury, with levels ranging  
72 from 4.8 to 18.4 ng m<sup>-3</sup> (Liu et al., 2002; Chen et al., 2013; Xiang and Liu, 2008; Fang et al., 2004). Similarly, South Asia has  
73 serious problems of environmental pollution due to elevated mercury emissions (UNEP, 2013), resulting in hazardous mercury



74 levels reported in water, lake sediment and fish samples (Karunasagar et al., 2006; Parvathi et al., 2010; Subramanian, 2004).  
75 In recent years, China and India signed the Minamata Convention and have started to control mercury emissions more strictly  
76 (Selin, 2014). Wu et al. (2017) stated that atmospheric mercury emissions from iron and steel production decreased from 35.6  
77 Mg in 2013 to 32.7 Mg in 2015, and Pacyna et al. (2010) estimated that total mercury emissions in China would decrease from  
78 635 Mg in 2005 to 290–380 Mg in 2020. Burger et al. (2013) estimated that total mercury emissions in India would increase  
79 from 310 Mg in 2010 to 540 Mg in 2020. In the context of serious mercury pollution and fast changes of regional mercury  
80 emission, atmospheric mercury observations in background sites within and near these mercury pollution concentrated regions  
81 can provide a scientific basis for evaluating the extent of mercury pollution and for informing public policy.

82 Located between South Asia and East Asia, the Tibetan Plateau is a vast high altitude landform featured by remote and  
83 pristine environments. There are limited local anthropogenic activities and previous studies reported that the atmospheric  
84 environment of the Tibetan Plateau remains global background levels (Fu et al., 2012a; Sheng et al., 2013; Xiao et al., 2012).  
85 However, historical records from ice core and lake sediments suggested that the Tibetan Plateau is an important part of global  
86 mercury cycle (Kang et al., 2016; Yang et al., 2010). Further, it has been increasingly perceived that the inland of Tibetan  
87 Plateau can be influenced by trans-boundary air pollution such as black carbon originating from the surroundings especially  
88 South Asia by crossing the Himalayas (Xia et al., 2011; Cong et al., 2015; Wan et al., 2015; Li et al., 2016). Studies of mercury  
89 in precipitation and water vapor evidenced that the Tibetan Plateau is likely sensitive to pollutant input including mercury  
90 (Huang et al., 2012; Huang et al., 2016), and the particulate-bound mercury in total suspended particulates was found at high  
91 concentrations in Lhasa which were comparable to other cities in China (Huang et al., 2016). A few measurements of  
92 atmospheric mercury at sites on the fringes of the Tibetan Plateau reported TGM concentrations in the range of 1.98–3.98 ng  
93 m<sup>-3</sup> (Fu et al., 2012a; Fu et al., 2008; Zhang et al., 2015), which were slightly higher than the northern hemispherical  
94 background level, implying possible impact of anthropogenic emissions. The Nam Co Station, an inland site in the Tibetan  
95 Plateau, is an ideal site to determine the TGM of the inland Tibetan Plateau because it is rarely affected by locally anthropogenic  
96 emission of mercury.

97 In this study, high-time resolution TGM was measured at the Nam Co Station from January 2012 to October 2014 and  
98 the temporal characteristics of atmospheric mercury were studied. Comparison with meteorological data, Multiple Linear



99 Regression (MLR) and a box model were used to investigate the temporal mercury variations at the Nam Co Station. HYSPLIT  
100 (HYbrid Single-Particle Lagrangian Integrated Trajectory), WRF-FLEXPART (FLEXible PARTicle dispersion model) and  
101 Potential Source Contribution Function (PSCF) were used to identify potential sources and impacts from long-range transport.  
102 The objective of this study is to (1) summarize the levels and temporal characteristics of TGM at a remote site in the inland  
103 Tibetan Plateau in a long-term measurement, (2) identify potential source regions of TGM at the Nam Co Station and (3)  
104 provide in-situ observational constraint that may contribute to understand changes in Asian mercury pollution.

## 105 **2 Measurements and Methods**

### 106 **2.1 Measurement site**

107 The Tibetan Plateau, with an average elevation of more than 4000 m, is known as the ‘Third Pole’ (Yao et al., 2012). Due  
108 to its low population and low level of industrialization, the inland of the Tibetan Plateau is minimally influenced by local  
109 emission sources and is regarded as an ideal natural laboratory for background atmospheric mercury monitoring.

110 The Nam Co comprehensive observation and research station (namely the Nam Co Station, 30°46.44′ N, 90°59.31′ E,  
111 and 4730 m a.s.l.) is a remote site between Nam Co Lake and the Nyainqêntanglha mountain range (Fig. 1). The Nam Co  
112 Station has been established since 2005 for maintaining a long-term record of the meteorological, ecological, and atmospheric  
113 measurements in the Tibetan Plateau (Cong et al., 2007; Li et al., 2007; Kang et al., 2011; Huang et al., 2012; Liu et al., 2015;  
114 de Foy et al., 2016b). There are restricted point sources of anthropogenic mercury emissions nearby the Nam Co Station.  
115 Dangxiong County is the nearest town on the southern slopes of the Nyainqêntanglha mountain range approximately 60 km  
116 south from Nam Co and Dangxiong is about 500 m lower than the Nam Co Station. Nomadism and tourism are the only human  
117 activity mostly during summer. Lhasa, the largest city in Tibet, is ~125 km south of the Nam Co Station.

118 TGM measurements were conducted at the Nam Co Station starting on January 15, 2012 until October 4, 2014 (Fig. S1).  
119 Field operators checked the instruments and created a monitoring log file each day at the Nam Co Station. Measurements were  
120 intermittently interrupted because of equipment maintenance and unstable power supply due to damage from strong winds to  
121 the electrical wires at the Nam Co Station. All data displayed in this study are in UTC+8 and solar noon at the Nam Co Station  
122 is at 13:56 in UTC+8 (China Standard Time, Beijing Time).



123        **2.2 Measurements: TGM, surface ozone and meteorology**

124        Measurements of TGM concentrations were performed with a Tekran model 2537 B instrument (Tekran Instruments Corp.,  
125 Toronto, Ontario, Canada). The Tekran 2537 B was installed in the monitoring house at the Nam Co Station and ambient air  
126 was introduced from the inlet which was 1.5 m above the roof and 4 m above the ground. A 45-mm diameter Teflon filter (pore  
127 size 0.2  $\mu\text{m}$ ) was placed in front of the inlet. The Tekran 2537 B measurements are based on the amalgamation of mercury  
128 onto a pure gold surface. By using a dual cartridge design, continuous measurements of mercury in the air can be made. The  
129 amalgamated mercury was thermally desorbed into an argon carrier gas stream and analyzed using an internal detector which  
130 was designed by cold vapor atomic fluorescence spectrophotometry ( $\lambda=253.7\text{nm}$ ) (Landis et al., 2002) providing TGM analysis  
131 at sub-ng  $\text{m}^{-3}$  levels. The sampling interval of the Tekran 2537 B was 5 min and the sampling flow rate was 0.8  $\text{L min}^{-1}$  (at  
132 standard temperature and pressure). The Tekran 2537 B was calibrated automatically every 25 hours using the internal mercury  
133 permeation source and was calibrated manually using a Tekran 2505 randomly 1-2 times a year.

134        Surface ozone was measured as a surrogate measure of oxidizing potential of the atmosphere (Stamenkovic et al., 2007)  
135 at the Nam Co Station using a UV photometric instrument (Thermo Environmental Instruments, USA, Model 49i) which uses  
136 absorption of radiation at 254 nm and has a dual cell design. The monitor was calibrated using a 49i-PS calibrator (Thermo  
137 Environmental Instruments, USA) before measurements and using aperiodic calibration during the monitoring periods. Details  
138 and analysis of the surface ozone measurements at the Nam Co Station were reported in Yin et al. (2017).

139        Measurements of temperature (T), relative humidity (RH), wind speed (WS), wind direction (WD) and downward  
140 shortwave radiation (SWD) were conducted at the Nam Co Station by a local weather station system (Milos 520, Vaisala Co.,  
141 Finland) and a radiation measurement system (CNR1, Kipp & Zonen Co., US), respectively (Ma et al., 2008).

142        **2.3 Meteorological simulations**

143        Gridded meteorological data for backward trajectories were obtained from the Global Data Assimilation System (GDAS-  
144 1) of the U.S. National Oceanic and Atmospheric Administration (NOAA) with  $1^\circ \times 1^\circ$  latitude and longitude horizontal  
145 resolution and vertical levels of 23 from 1000 hPa to 20 hPa (<http://www.arl.noaa.gov/gdas1.php>).

146        Backward trajectories and clusters were calculated using the NOAA-HYSPLIT model (Draxler and Rolph, 2003,



147 <http://ready.arl.noaa.gov/HYSPLIT.php>) using TrajStat (Wang et al., 2009), which is a free software plugin of MeteInfo  
148 (Wang, 2014). The backward trajectories arrival height in HYSPLIT was set at 500 m above the surface and the total run times  
149 was 120 hours for each backward trajectory. Trajectory positions were stored at time intervals of 3 hours. Angular distance  
150 was chosen to calculate clusters in HYSPLIT calculation.

151 In addition to HYSPLIT, WRF-FLEXPART (Brioude et al., 2013) was used to obtain clusters of particle trajectories  
152 reaching the Nam Co Station. 1000 particles were released per hour in the bottom 100 m surface layer above the Nam Co  
153 Station and were tracked in backward mode for 4 days (de Foy et al., 2016b). Residence Time Analysis (RTA) (Ashbaugh et  
154 al., 1985) was utilized to show the dominant transport paths of air masses impacting the samples (Wang et al., 2016; Wang et  
155 al., 2017). Six clusters were found to represent the prevailing flow patterns to the Nam Co Station simulated using WRF-  
156 FLEXPART.

#### 157 **2.4 Multiple linear regression model and box model**

158 A MLR model was used to quantify the main factors affecting the hourly concentrations of TGM. The method follows  
159 the description provided in de Foy et al. (2016a; 2016c) and de Foy (2017) and was used to analyze surface ozone  
160 concentrations at the Nam Co Station (Yin et al., 2017). The inputs to the MLR model include meteorological parameters  
161 (wind speed, temperature, solar radiation and humidity), surface ozone, inter-annual variation factors, seasonal factors, diurnal  
162 factors, WRF boundary layer heights, WRF-FLEXPART trajectory clusters and a CAMx stratospheric ozone tracer (see Yin et  
163 al. (2017) for more details). The inputs to the model were normalized linearly. An Iteratively Reweighted Least Squares (IRLS)  
164 procedure was used to screen for outliers. Measurement times when the model residual was greater than two standard  
165 deviations of all the residuals were excluded from the analysis. This was repeated iteratively until the method converged on a  
166 stable set of outliers. The variables to be included in the regression were obtained iteratively. At each iteration, the variable  
167 leading to the greatest increase in the square of Pearson's correlation coefficient was added to the inputs as long as the increase  
168 was greater than 0.005.

169 The distribution of TGM concentrations is approximately normal (see details in section 3.1), and so a linear model was  
170 used. TGM was scaled linearly to have a mean of 0 and a standard deviation of 1 in the regression model. A Kolmogorov-



171 Zurbenko filter (Rao et al., 1997) was used to separate the time series of specific humidity and temperature into a synoptic  
172 scale signal ( $> 3$ -5 days) and a diurnal scale signal using 5 passes of a 13-point moving average. Only the synoptic scale signal  
173 was included in the final regression results, as the diurnal variation was characterized by the other variables in the analysis.  
174 The other meteorological parameters used were the 24-hour average boundary layer height from WRF and the 8-hour local  
175 measured wind speeds (4 directions, 5 wind speed segments for a total of 20 factors corresponding to different wind speeds  
176 from different wind directions). The 24-hour average of ozone measurements (log-transformed) contributed to the model. In  
177 addition, a seasonal K-Z filtered time series of a CAMx tracer for transport from the free troposphere (above 300 hPa) to the  
178 surface contributed to the model.

179 A diurnal box model was used to investigate the diurnal variation of TGM at the Nam Co Station as was done for reactive  
180 mercury at the same site (de Foy et al., 2016b). Preliminary tests of the box model were made using solar radiation and  
181 temperature to represent chemical transformations, as well as using wind speed and boundary layer height to represent dilution.  
182 However these attempts failed to reproduce the diurnal variation found in the measurements. A simplified model that  
183 represented the diurnal variations was found by combining the following 5 inputs: TGM emissions at sunrise and in the early  
184 evening, constant TGM deposition 24 hours a day, a constant lifetime for TGM loss during daylight hours and TGM dilution  
185 due to vertical mixing.

## 186 **2.5 Anthropogenic mercury emissions and fire hot spots distribution**

187 The mercury emission inventory of China was obtained from Wu et al. (2016), which used a technology-based approach  
188 to compile a comprehensive estimate of Chinese provincial emissions for all primary anthropogenic sources. The emissions  
189 over other Asian countries were from UNEP global anthropogenic emission inventory (AMAP/UNEP, 2013). These inventories  
190 were for the year 2010 and had a horizontal resolution of  $0.5 \times 0.5^\circ$ .

191 MODIS fire spots were obtained from Fire Information for Resource Management System (FIRMS) operated by the  
192 National Aeronautics and Space Administration (NASA) of the United States (Giglio et al., 2003; Davies et al., 2004).

## 193 **2.6 Potential Source Contribution Function (PSCF)**

194 PSCF assumes that back-trajectories arriving at times of higher mixing ratios likely point to the more significant source





195 directions (Ashbaugh et al., 1985). PSCF has been applied in previous studies to locate sources of TGM for different sites (Fu  
196 et al., 2012a; Fu et al., 2012b; Zhang et al., 2015). The PSCF values for the grid cells in the study domain are based on a count  
197 of the trajectory segment (hourly trajectory positions) that terminate within each cell (Ashbaugh et al., 1985). Let  $n_{ij}$  be the  
198 total number of endpoints that fall in the  $ij$ th cell during whole simulation period. Let  $m_{ij}$  represents the number of points in  
199 the same cell that have arrival times at the sampling site corresponding to TGM concentrations higher than a set criterion. In  
200 this study, we calculate the PSCF based on trajectories corresponding to concentrations that exceed the mean level ( $1.33 \text{ ng m}^{-3}$ )  
201 of TGM. The PSCF value for the  $ij$ th cell is then defined as:

$$202 \quad \text{PSCF}_{ij} = m_{ij}/n_{ij}$$

203 The PSCF value can be interpreted as the conditional probability that the TGM concentration at measurement site is  
204 greater than the mean mixing ratios if the air parcel passes through the  $ij$ th cell before arriving at the measurement site. In cells  
205 with high PSCF values are associated with the arrival of air parcels at the receptor site that have TGM concentrations that  
206 exceed the criterion value. These cells are indicative of areas of ‘high potential’ contributions for the chemical constituent.

207 Identical  $\text{PSCF}_{ij}$  values can be obtained from cells with very different counts of back-trajectory points (e.g. grid cell A  
208 with  $m_{ij}=5000$  and  $n_{ij}=10000$  and grid cell B with  $m_{ij} = 5$  and  $n_{ij} = 10$ ). In this extreme situation grid cell A has 1000 times  
209 more air parcels passing through than grid cell B. Because of the sparse particle count in grid cell B, the PSCF values are more  
210 uncertain and the contribution from B is limited. To account for the uncertainty due to low values of  $n_{ij}$ , the PSCF values were  
211 scaled by a weighting function  $W_{ij}$  (Polissar et al., 1999). The weighting function reduced the PSCF values when the total  
212 number of the endpoints in a cell was less than about three times the average value of the end points per each cell. In this case,  
213  $W_{ij}$  was set as follows:

$$214 \quad W_{ij} = \begin{cases} 1.00 & n_{ij} > 3N_{ave} \\ 0.70 & 3N_{ave} > n_{ij} > 1.5N_{ave} \\ 0.42 & 1.5N_{ave} > n_{ij} > N_{ave} \\ 0.05 & N_{ave} > n_{ij} \end{cases} \quad (1)$$

215 where  $N_{ave}$  represents the mean  $n_{ij}$  of all grid cells. The weighted PSCF values obtained by multiplying the original PSCF  
216 values by the weighting factor: weighted PSCF result= $W_{ij} \times \text{PSCF}$ .

### 217 **3 Results and discussion**



### 218 3.1 TGM concentrations

219 The mean TGM concentration at the Nam Co Station is  $1.33 \pm 0.24 \text{ ng m}^{-3}$ , which is the lowest among all reported TGM  
220 concentrations at remote sites in China and is much lower than all urban sites in China (Fu et al., 2012a; Fu et al., 2012b; Fu  
221 et al., 2011; Fu et al., 2010; Fu et al., 2008; Zhang et al., 2013; Zhu et al., 2012; Zhang et al., 2015). The mean concentration  
222 of TGM is slightly lower than the annual mean concentration at background sites in the Northern Hemisphere ( $1.55 \text{ ng m}^{-3}$  in  
223 2013 and  $1.51 \text{ ng m}^{-3}$  in 2014), and higher than those in the Southern Hemisphere ( $0.93 \text{ ng m}^{-3}$  in 2013 and  $0.97 \text{ ng m}^{-3}$  in  
224 2014) (Sprovieri et al., 2016). Comparable results were reported from EvK2CNR on the south slope of the Himalayas ( $1.2 \text{ ng}$   
225  $\text{m}^{-3}$ , Gratz et al., 2013), and from tropical sites in the Global Mercury Observation System in the Northern Hemisphere ( $1.23$   
226  $\text{ng m}^{-3}$  in 2013 and  $1.22 \text{ ng m}^{-3}$  in 2014) (Sprovieri et al., 2016). Comparing to the three sites at the edge of the Tibetan Plateau  
227 (Mt. Waliguan, Shangri-La and Mt. Gongga, Table S1), the mean TGM concentration at the Nam Co Station was substantially  
228 lower, indicating that the inland Tibetan Plateau has a more pristine environment than the edges of the plateau.

229 The frequency distribution of TGM at the Nam Co Station was normally distributed (Fig. 2). 81% of hourly average TGM  
230 concentrations were in the range of  $1.0\text{-}1.6 \text{ ng m}^{-3}$  with few episodically elevated TGM and low TGM concentrations. 1.6%  
231 ( $n=236$ ) out of all hourly mean TGM data ( $n=14408$ ) were greater than  $1.81 \text{ ng m}^{-3}$  (overall mean TGM +  $2 \times \text{SD}$ , namely  
232  $1.33 + 2 \times 0.24 = 1.81$ ), and 1.5% ( $n=213$ ) were lower than  $0.85 \text{ ng m}^{-3}$  (overall mean TGM -  $2 \times \text{SD}$ , namely  $1.33 - 2 \times 0.24 = 0.85$ ).

233 The monthly average TGM at the Nam Co Station showed a weak decreasing trend (slope =  $-0.006$ ) during the entire  
234 monitoring period, and the decrease was more pronounced in the intra-annual variability in the summer (slope =  $-0.013$ ). The  
235 slight decreasing trend of TGM at the Nam Co Station was in agreement with a recent study using plant biomonitoring to  
236 identify a decreasing atmospheric mercury since 2010 near Dangxiong county (Tong et al., 2016) as well as a worldwide  
237 downward trend of TGM (Slemr et al., 2011; Zhang et al., 2016).

### 238 3.2 Seasonal variations of TGM

239 In contrast with many previous observations in China (Zhang et al., 2015; Fu et al., 2008b; Fu et al., 2009; Fu et al., 2010;  
240 Fu et al., 2011; Fu et al., 2012b; Feng et al., 2004; Xiu et al., 2009; Xu et al., 2015; Wan et al., 2009) and most AMNet  
241 (Atmospheric Mercury Network) sites (Lan et al., 2012), TGM at the Nam Co Station shows a seasonal variation with a  
242 maximum in the summer (June, July and August) and a minimum in the winter (December, January and February) (Fig. 3).



243 The seasonal mean TGM values decreased in the following order: summer ( $1.50 \pm 0.20 \text{ ng m}^{-3}$ ) > spring ( $1.28 \pm 0.20 \text{ ng m}^{-3}$ ) >  
244 autumn ( $1.22 \pm 0.17 \text{ ng m}^{-3}$ ) > winter ( $1.14 \pm 0.18 \text{ ng m}^{-3}$ ) (Table 1). The highest monthly mean TGM concentration of  $1.54 \text{ ng m}^{-3}$   
245  $\text{m}^{-3}$  in July was  $0.43 \text{ ng m}^{-3}$  higher than the lowest of  $1.11 \text{ ng m}^{-3}$  in November.

246 Measurements of TGM in other sites in the Tibetan Plateau also reported diverse seasonal patterns (Fig. 4). For example,  
247 Fu et al. (2012a) found that at Waliguan the maximum TGM concentration was in January 2008, resulting from long-range  
248 transport of pollutions from Northern India. Aside from January, monthly mean TGM concentrations at Waliguan had a clear  
249 trend with high levels in warm seasons, and lower levels in cold seasons. The TGM variation at Mt. Gongga (Fu et al., 2008)  
250 had a minimum in the summer, possibly due to the accelerated oxidation followed by dry deposition and wet scavenging  
251 processes in the summer. The winter maximum of TGM at Mt. Gongga (Fu et al., 2008) implied the impact from anthropogenic  
252 mercury emissions in the cold months. The seasonal variation of TGM at Shangri-La (Zhang et al., 2015) had high levels in  
253 the spring and autumn, and low levels in the summer and winter which was different from all the other sites in the Tibetan  
254 Plateau.

255 Comparing to the other high altitude background sites in mid-latitudes in Europe (Fig. 5) (Denzler et al., 2017; Fu et al.,  
256 2016a; Ebinghaus et al., 2002) and sites in mid-latitudes in the US (Holmes et al., 2010; Weiss-Penzias et al., 2003; Sigler et  
257 al., 2009; Yatavelli et al., 2006), the lower concentration of TGM at the Nam Co Station in the winter might be indicative of  
258 atmospheric mercury depletion in the winter caused by reactive halogens. The reaction rates for these reactions are a strong  
259 inverse function of temperature (de Foy et al., 2016b), and they are accompanied by lower surface ozone concentration (Yin  
260 et al., 2017), which is catalytically destroyed by halogens (Bottenheim et al., 1986; Obrist et al., 2011).

261 The summer peak of TGM at the Nam Co Station may be related to both the local re-emission of mercury from the earth's  
262 surface, and the long range transport of mercury from South Asia (see details in section 3.6). At the Nam Co Station, daily  
263 mean TGM had a correlation coefficient with daily mean temperature reaching 0.56. Higher temperature in the warm seasons  
264 (Fig. 6) might lead to remobilization of soil mercury re-emission, which has been evidenced by a recent study on surface-air  
265 mercury exchange in the northern Tibetan Plateau (Ci et al., 2016). It is also possible that weaker wind speeds during the warm  
266 season (Fig. 6) suppressed the dilution of TGM with fresh air aloft in a low boundary layer. Furthermore, most precipitation  
267 happens in the summer at the Nam Co Station (You et al., 2007) and can increase emission of mercury from the Earth's surface



268 by physical displacement of interstitial soil air by the infiltrating water (Ci et al., 2016) and by additional input of mercury  
269 from wet deposition (Huang et al., 2012). Besides local emissions, the summer monsoon can facilitate the transport of air  
270 masses with higher TGM concentrations from South Asia, and hence may also contribute to the summer peak of TGM.

271 The month of April in both 2012 and 2013 had higher monthly TGM levels than the months before and after (Fig. S1),  
272 possibly resulting from mercury emission from Nam Co Lake as the lake started to thaw in April (Gou et al., 2015).

### 273 **3.3 Diurnal variations of TGM**

274 Diurnal variations of TGM in different seasons exhibited a regular pattern, characterized by a sharp rise shortly after  
275 sunrise and a fairly steady decrease from the morning peak until sunset (Fig. 7). After sunset, TGM increased until midnight  
276 in the summer, the spring and the autumn. The diurnal variation of TGM at the Nam Co Station was similar to those of Mt.  
277 Gongga (Fu et al., 2009), Mt. Leigong (Fu et al., 2010), Mt. Changbai (Fu et al., 2012b), Mt. Waliguan (Fu et al., 2012a) and  
278 Reno (Peterson et al., 2009) except that the morning increase occurs earlier and is shorter compared during other sites that  
279 have a gradual increase throughout the morning.

280 Fig. 8 showed the comparison of TGM concentrations with a box model simulation by season. The best match in the box  
281 model was obtained by using variables including constant TGM deposition throughout the day, TGM emissions at sunrise,  
282 TGM emissions in the early evening, TGM dilution due to vertical mixing and lifetime of TGM loss during daylight hours  
283 (Table 2). The  $R^2$  of the model simulation ranged from 0.91 to 0.99, suggesting that the simulations reproduced the diurnal  
284 variations reliably. As described above, both the measurements and the model have sharp bursts of TGM in the morning (7:00-  
285 9:00) and in the evening (18:00-22:00) during all seasons. Constant depletion existed in the spring, summer and autumn which  
286 would correspond to deposition rates of around 1 to 2  $\text{ng m}^{-2} \text{h}^{-1}$ .

287 Fig. 9 showed the seasonal diurnal profiles of TGM and meteorological parameters. TGM concentrations were stable or  
288 slightly decreasing after midnight (0:00-6:00) under shallow nocturnal boundary layers. Notably, the morning increase of TGM  
289 happens immediately after sunrise, but before the increases of temperature, wind speed or humidity. The atmospheric mercury  
290 bursts in the morning (7:00-9:00) is probably due to prompt re-emission of nocturnal mercury deposition on the Earth's surface  
291 (Fu et al., 2016b; Howard et al., 2017; Howard et al., 2017; Kim 2010). The stable nocturnal boundary layer terminated at  
292 sunrise at which point mercury, including the mercury in the soil indigenously and/or deposited overnight, started to be



293 reemitted into the shallow stable boundary layer before the increase of temperature which leads to an increase in the mixing  
294 height. As the temperature and radiation increased, so did the boundary layer height which developed into a convective mixed  
295 boundary layer and generated greater vertical mixing between the surface air and the air loft. At the same time, surface wind  
296 speed also increased. With increased vertical and horizontal dispersion, TGM released from the surface was diluted during the  
297 daytime (Liu et al., 2011; Lee et al., 1998). The higher surface ozone concentration and SWD during the daytime (Fig. 9) may  
298 also have promoted the formation of atmospheric oxidants and the transition from GEM to RGM and subsequent deposition  
299 or scavenging, resulting in depletion of atmospheric mercury. This is evidenced by the increasing RGM concentrations  
300 observed in the afternoon at Nam Co in a different study (de Foy et al., 2016b). When the temperature decreased and the  
301 boundary layer converted back into a nocturnal boundary layer after sunset, depressed vertical mixing facilitated the build-up  
302 of TGM and such build-up was more significant in the warm seasons. In the evening, increases in TGM correspond to increases  
303 in specific humidity, especially in the summer.

#### 304 **3.4 Multiple linear regression and WRF-FLEXPART clusters results**

305 Results of the MLR simulations for the entire measurement period (2012-2014) had a close correlation with the  
306 measurements: the correlation coefficient was 0.77 for all 12649 data points and 0.84 excluding the 383 outliers (Fig. 10). The  
307 primary contributor to the variance of the simulated time series was the seasonal signal, including the 12-month and 6-month  
308 harmonics as well as the smoothed specific humidity and temperature time series (Table 3). These were grouped together when  
309 presenting the results because they were not orthogonal to each other, and they contributed 84% of the variance of TGM in  
310 MLR simulation. The diurnal factors accounted for 4% of the variance, the WRF boundary layer heights accounted for 4% of  
311 the variance, and the local winds were associated with 1% of the variance. These factors show that there is an impact from  
312 horizontal and vertical dispersion as well as daily cycling patterns due to either transport or chemistry, but that these factors  
313 are considerably smaller than the seasonal variation at the site. Only 1% of the variance was associated with the annual signal,  
314 showing that the downward trend in the concentrations reported in Sec. 3.1 was a small contributor to variations in TGM at  
315 Nam Co. The time series of surface ozone concentration contributed 3% to the variance and the stratospheric ozone tracer  
316 contributed 3%. We hypothesize that this is because ozone concentrations act as an indicator of the oxidative potential of the  
317 air mass, although in the case of surface ozone concentration it could also be because they are a tracer of aged polluted air



318 masses.

319 The regression analysis screens for high and low outliers. In particular, high outliers are significant in terms of TGM  
320 concentrations: they have an average concentration of  $1.91 \text{ ng m}^{-3}$  which is  $0.58 \text{ ng m}^{-3}$  higher than the average of the  
321 measurements retained in the simulations (Fig. 10). The middle panel in Fig. 10 shows that a number of the high outliers are  
322 associated with specific peak events, indicating that occasional plumes of high TGM are not associated with recurring  
323 emissions or periodically occurring conditions. A significant amount of TGM not accounted-for in the model is due to the high  
324 outliers. Additionally, a few events with very low TGM concentrations are not simulated. Fig. 11a shows the 6 wind transport  
325 clusters based on the hourly WRF-FLEXPART simulations. The figure shows the average residence time analysis for all the  
326 hours in each cluster, which characterizes the path of the air masses arriving at the measurement site for each cluster. The most  
327 frequent clusters are clusters 1 and 2 which account for 30% and 34% of measurement hours respectively. For measurement  
328 times during these clusters, the air masses clearly come from the west with a slight southern component for cluster 1 and a  
329 slight northern component in the case of cluster 2. Cluster 3 represents hours influenced by transport from the north which  
330 occurred during 15% of the measurement period. These are associated with the passage of storms at Nam Co: as the low  
331 pressure system moves to the east, the winds shift from northwesterly to northeasterly. Clusters 4, 5 and 6 occur less frequently  
332 and all represent different types of wind transport across the Himalayas from the south. Cluster 4 was the least frequent cluster,  
333 occurring 5% of the time. It includes transport from the southeast including the northeastern corner of the Indo-Gangetic plain  
334 and occasional transport from southwestern China. This cluster also includes transport from the direction of Lhasa. Cluster 5  
335 occurred 7% of the time and represents transport from the south including Bangladesh. Cluster 6 occurred 9% of the time and  
336 included transport from Nepal and northern India.

337 The WRF-FLEXPART clusters were included in the MLR analysis and helped to improve the simulations for several  
338 tests. However, they did not increase the correlation coefficient of the final regression time series and consequently were not  
339 included in the final MLR results. This could be because transport is already characterized by the other variables in the model  
340 such as temperature and humidity (which can serve as tracers of different air masses) and local wind speed and direction.  
341 Nevertheless, the importance of air mass transport can be seen from the probability density function of the TGM concentrations  
342 by cluster shown in Fig. 11b. Clusters 1 and 2, which have transport from the west, clearly have the lowest TGM concentrations.



343 Next in terms of increasing TGM concentrations are clusters 3 and 6 which have transport from the north and from the  
344 southwest. The highest concentrations are very clearly associated with cluster 4 which has transport from the east and through  
345 Lhasa. Of the 87 hours with concentrations higher than  $2 \text{ ng m}^{-3}$ , 59% occur during cluster 4 and 17% during cluster 5 with  
346 less than 8% for each of the other clusters. This demonstrates clearly that in addition to having the highest average levels,  
347 clusters 4 and 5 account for most of the peak concentrations.

### 348 **3.5 Anthropogenic and natural sources of TGM**

349 Sources of atmospheric mercury can be simply divided into natural sources and anthropogenic sources. China was the  
350 biggest anthropogenic mercury emitter in Asia with a large fraction of emissions from coal combustion (Pirrone et al., 2010)  
351 mostly distributed in the eastern and central part of China (Fig. S2). Anthropogenic mercury emissions in South Asia were  
352 mostly in the Indo-Gangetic Plain (IGP) including most of northern and eastern India, the eastern parts of Pakistan, and all of  
353 Bangladesh (Fig. S2) all of which have high population density and many industrial centers. For the Tibetan Plateau itself,  
354 there was no obvious anthropogenic mercury emissions in Tibet except Lhasa city (Fig. S2).

355 Biomass burning is the largest natural source of atmospheric mercury on land especially for TGM/GEM (Pirrone et al.,  
356 2010) and can lead to high TGM concentration events at sites far from the emissions (de Foy et al., 2012). Fire hot spots  
357 distribution were used in this study to indicate the biomass burning in Asia during the whole measurement period (Fig. S3).  
358 Plenty of fire hot spots were observed in the regions surrounding the Tibetan Plateau including the IGP, the Indo-China  
359 Peninsula and southeastern China while few were found in the Tibetan Plateau. Central Asia countries such as Kyrgyzstan and  
360 Tajikistan also had many fire hot spots with simultaneous passing trajectories. Previous studies have proved that carbonaceous  
361 aerosols from biomass burning in the IGP can reach the inland Tibetan Plateau by crossing the Himalayas (Cong et al., 2015),  
362 and further influence the inland Tibetan Plateau. Therefore, atmospheric mercury originating from biomass burning in South  
363 and Central Asia may contribute to TGM at the Nam Co Station.

364 Re-emissions are a result of natural processes when mercury previously deposited from air onto soils, surface waters and  
365 vegetation can be re-emitted back to the atmosphere (UNEP, 2013). These emissions of “old” mercury can be from both natural  
366 sources and anthropogenic sources. Field measurements and controlled field experiments at Beiluhe Station (Ci et al., 2016)  
367 in the central Tibetan Plateau indicated that the surface soils were high emitters of mercury during warm seasons but were net



368 sinks in the winter due to deposition. Furthermore, diurnal air-surface exchange showed that soils were net emitters in the  
369 daytime and net sinks at night (Ci et al., 2016). The diurnal variation of TGM at the Nam Co Station and the box model results  
370 (Sec. 3.3) suggest that Beiluhe and Nam Co probably have similar re-emission patterns.

### 371 **3.6 HYSPLIT and PSCF results**

372 Backward trajectories were calculated using HYSPLIT to identify the origins of air masses and associated TGM  
373 concentrations to the Nam Co Station. Results of air masses at different heights (500m, 1000m and 1500m) showed similar  
374 patterns, hence, we selected trajectories released at a height of 500 m as representative since 500 m is suitable for considerations  
375 of both the long-range transport and transport in the planetary boundary layer. Fig. 12 showed the result of clusters analysis  
376 based on the HYSPLIT backward trajectories during the whole measurement period at the Nam Co Station. Most trajectories  
377 originated from the west of Nam Co including the western and central Tibetan Plateau, southwestern of the Xinjiang Uygur  
378 Autonomous Region, South Asia, Central Asia and Western Asia, very few trajectories originated from eastern China. The  
379 backward trajectories were grouped into 6 clusters. Cluster 3 indicated the air mass from the south, originating from Bhutan  
380 and Bangladesh. This cluster had the lowest starting heights as well as traveling heights, but the highest mean TGM  
381 concentration ( $1.48 \text{ ng m}^{-3}$ ) (Table S2) in agreement with the FLEXPART results (Sec. 3.4). Clusters 1, 2, 4, 5 and 6 originated  
382 in the west, including air masses originating from northern India, Pakistan, Afghanistan and Iran passed over the Himalayas  
383 before arriving at the Nam Co Station. They had longer pathways through the Tibetan Plateau than Cluster 3. Cluster 4 had the  
384 longest transport route from the west, suggestive of faster wind speeds, and also the lowest TGM mean concentration ( $1.12 \text{ ng}$   
385  $\text{m}^{-3}$ ) with relatively high transport height.

386 PSCF calculations were based on concurrent TGM measurements and HYSPLIT backward trajectories, and thus can  
387 further constrain the potential source regions. As shown in Fig. 13, IGP, the southern Xinjiang Uygur Autonomous Region, the  
388 western Qinghai province and areas near the Nam Co Station in Tibet Autonomous Region were identified as overall high  
389 potential sources regions and pathways. Except for the areas near the Nam Co Station, these potential sources regions  
390 correspond well with the atmospheric mercury emissions and biomass burning distributions displayed in Sec. 3.5. The Bay of  
391 Bengal was identified as a potential source region probably due to high emissions from its surroundings associated with  
392 frequent occurrence of trajectories passing through this area in the summer.





393 Seasonal PSCFs were calculated in 2012 to investigate the potential sources by season (Fig. 14). In the spring, the autumn  
394 and the winter, the Nam Co Station was dominated by the Westerlies. Pollutants from South Asia might be diluted by the clean  
395 air during the transport within the Tibetan Plateau before they arrived at the Nam Co Station (Fig. S4). A zonal region in the  
396 central IGP (Fig. 14) with elevated pollution represents a constant potential source (Gautam et al., 2011; Mallik and Lal, 2014).  
397 The significant impact of long-range transport pollution from northwestern India on the Tibetan Plateau was also evidenced  
398 by TGM measurements at Waliguan (Fu et al., 2012a). In the summer, the Indian Monsoon prevails and air masses arrived at  
399 the Nam Co Station that had shorter pathway after entering the Tibetan Plateau than those in other seasons (Fig. S4). The  
400 central IGP was again found to have higher PSCF values than other regions, even though these were much lower than the  
401 PSCF values of other seasons. The highest PSCF values in the summer were in the eastern IGP (Fig. 14). For all seasons, the  
402 region near the Nam Co Station, especially its south and west, was high in PSCF values all through the year, indicating that  
403 air masses with high TGM concentrations predominantly came from the south-southwest.

### 404 **3.7 Implications for transboundary air pollution to the Tibetan Plateau**

405 The seasonal atmospheric circulation patterns in the Tibetan Plateau is characterized by the Indian monsoon in the summer  
406 and the Westerlies in the winter. Such a climate regime exerts a profound impact on the seasonal atmospheric environment by  
407 affecting the air transport dynamic and associated climate conditions. Pollutants like black carbon and hexachlorocyclohexanes  
408 peaked in pre-monsoon season and declined during monsoon season at Nam Co and Lulang, resulting from seasonal rainfall  
409 variations that can scavenge aerosols during their transport from source regions to the Tibetan Plateau (Zhang et al., 2017; Wan  
410 et al., 2015; Sheng et al., 2013). In contrast, gaseous pollutants showed different seasonal patterns: TGM at Nam Co in this  
411 study and persistent organic pollutants (dichlorodiphenyltrichloroethane and polychlorinated biphenyls) at Lulang showed  
412 higher concentrations during the monsoon season compared to the pre-monsoon season (Sheng et al., 2013). TGM at Nam Co  
413 showed strong covariance with temperature and specific humidity, all of which are in phase with the Indian Monsoon Index  
414 (IMI) (Wang and Fan, 1999; Wang et al., 2001) (Fig. 15), indicating the importance of Indian Summer Monsoon as a major  
415 driver delivering of transboundary transport of air pollution into the inland Tibetan Plateau. We suggest that gaseous pollutants  
416 are not readily deposited and/or washed out by precipitation during their transport and are more likely associated with the  
417 transport dynamics driven by the Indian Summer Monsoon, hence they showed high values when the Indian Summer Monsoon



418 prevails. Transboundary air pollution is not the sole factor contributing to elevated TGM during summer: temperature-  
419 dependent processes such as gas-particle fractionation and surface reemission can also contribute to such seasonal patterns.  
420 Nonetheless, the close relationship between TGM and the Indian Summer Monsoon and the clear difference in seasonal  
421 patterns between gaseous and particulate pollutants together indicate that additional measurements of multiple pollutants and  
422 comparative studies are required to achieve a more comprehensive understanding and assessment of transboundary air  
423 pollution to the Tibetan Plateau.

#### 424 **4 Conclusions**

425 We conducted three-years of TGM measurements at the Nam Co Station in the inland area of the Tibetan Plateau, China,  
426 from January 2012 to October 2014. The mean TGM concentration was  $1.33 \pm 0.24 \text{ ng m}^{-3}$  during the whole measurement  
427 period and the extremely low TGM level at the Nam Co Station indicated the pristine environment in the inland Tibetan Plateau.  
428 A weak decreasing trend of TGM was identified over the course of the measurements.

429 In contrast to many other sites in China, TGM at the Nam Co Station showed high concentrations in warm seasons and  
430 low concentrations in cold seasons. Compared with other high altitude background sites, the low concentration of TGM at the  
431 Nam Co Station in the winter may be due to the depletion of mercury. Seasonal variation of TGM at the Nam Co Station was  
432 influenced by factors such as re-emission processes of deposited mercury over the Earth's surfaces, vertical mixing and long-  
433 range transport. Multiple linear regression, backward trajectories and PSCF were investigated at the Nam Co Station and  
434 results indicated that long-range transports from the central and eastern Indo-Gangetic Plain were potentially the main sources  
435 for seasonally elevated TGM at the Nam Co Station due to the alternate impact of the Westerlies and of the Indian monsoon.

436 At the Nam Co Station, the diurnal TGM profile had a peak 2-3 hours after sunrise and reached its lowest concentration  
437 before sunset. The box model provided supporting evidence and estimates of diurnal TGM deposition and TGM bursts of  
438 (re)emissions at the Nam Co Station in addition to dilution due to vertical mixing. The background TGM variation at the Nam  
439 Co Station was jointly regulated by surface-air flux and dilution in the planetary boundary layer in the diurnal cycle. Daily  
440 meteorology conditions, such as high temperature, high solar radiation and more precipitation facilitated the Earth's surface  
441 mercury emission. The decline of TGM concentrations in the daytime was likely due to vertical dilution from increased vertical  
442 mixing, as well as due to the conversion of GEM to oxidized species that are easily deposited.



443 Due to the insolubility of TGM, which is different from particulate pollutant, TGM was less affected by the precipitation  
444 during the transport in monsoon season and measurement of TGM at the Nam Co Station can continually reflect the  
445 transboundary air pollution from the South Asia to the inland Tibetan Plateau.

446 The measurements of TGM at the Nam Co Station will be useful in providing atmospheric mercury baseline in the remote  
447 inland Tibetan Plateau, improving the accuracy of modeled concentrations of TGM in the inland Tibetan Plateau, and serving  
448 as new constraint for assessment of Asian mercury emission and pollution.

449

450 Data availability. All the data presented in this paper can be made available for scientific purposes upon request to the  
451 corresponding authors (Qianggong Zhang ([qianggong.zhang@itpcas.ac.cn](mailto:qianggong.zhang@itpcas.ac.cn)) or Shichang Kang ([shichang.kang@lzb.ac.cn](mailto:shichang.kang@lzb.ac.cn))).

452

#### 453 **Acknowledgements**

454 This study was supported by the National Natural Science Foundation of China (41630754, 41630748, 41721091) and  
455 Tianjin City Key Research & Development Plan (15YFYSSF00010). Q. G. Zhang acknowledges financial support from the  
456 Youth Innovation Promotion Association of CAS (2016070). X. F. Yin acknowledges China Scholarship Council. The authors  
457 are grateful to Yaqiang Wang, who is the developer of MeteoInfo and who provided generous help. The authors thank NOAA  
458 for providing the HYSPLIT model and GFS meteorological files. Finally, the authors would like to thank the editor and referees  
459 of this paper for their helpful comments and suggestions.

460

461

462

463

464

465

466

467

468 **References:**

- 469 AMAP/UNEP: Technical Background Report for the Global Mercury Assessment 2013, Arctic Monitoring and  
470 Assessment Programme, 2013.
- 471 Ashbaugh, L. L., Malm, W. C., and Sadeh, W. Z.: A residence time probability analysis of sulfur concentrations at  
472 Grand Canyon National Park, *Atmospheric Environment* (1967), 19, 1263-1270, 1985.
- 473 Assessment, U. G. M.: Sources, Emissions, Releases and Environmental Transport, UNEP Chemicals Branch, Geneva,  
474 Switzerland, 42, 2013.
- 475 Bottenheim, J., Gallant, A. G., and Brice, K. A.: Measurements of NO<sub>y</sub> species and O<sub>3</sub> at 82 N latitude, *Geophysical*  
476 *Research Letters*, 13, 113-116, 1986.
- 477 Brioude, J., Arnold, D., Stohl, A., Cassiani, M., Morton, D., Seibert, P., Angevine, W., Evan, S., Dingwell, A., and Fast,  
478 J. D.: The Lagrangian particle dispersion model FLEXPART-WRF version 3.1, *Geoscientific Model Development*, 6, 1889-  
479 1904, 2013.
- 480 Burger Chakraborty, L., Qureshi, A., Vadenbo, C., and Hellweg, S.: Anthropogenic mercury flows in India and impacts  
481 of emission controls, *Environmental science & technology*, 47, 8105-8113, 2013.
- 482 Chen, L., Liu, M., Xu, Z., Fan, R., Tao, J., Chen, D., Zhang, D., Xie, D., and Sun, J.: Variation trends and influencing  
483 factors of total gaseous mercury in the Pearl River Delta—A highly industrialised region in South China influenced by  
484 seasonal monsoons, *Atmospheric environment*, 77, 757-766, 2013.
- 485 Choi, H.-D., and Holsen, T. M.: Gaseous mercury emissions from unsterilized and sterilized soils: the effect of  
486 temperature and UV radiation, *Environmental Pollution*, 157, 1673-1678, 2009.
- 487 Ci, Z., Peng, F., Xue, X., and Zhang, X.: Air–surface exchange of gaseous mercury over permafrost soil: an  
488 investigation at a high-altitude (4700 m asl) and remote site in the central Qinghai–Tibet Plateau, *Atmospheric Chemistry*  
489 *and Physics*, 16, 14741-14754, 2016.
- 490 Cong, Z., Kang, S., Liu, X., and Wang, G.: Elemental composition of aerosol in the Nam Co region, Tibetan Plateau,  
491 during summer monsoon season, *Atmospheric Environment*, 41, 1180-1187, 2007.
- 492 Cong, Z., Kawamura, K., Kang, S., and Fu, P.: Penetration of biomass-burning emissions from South Asia through the  
493 Himalayas: new insights from atmospheric organic acids, *Scientific reports*, 5, 9580, 2015.
- 494 Davies, D., Kumar, S., and Descloitres, J.: Global Fire Monitoring Use of MODIS Near-real-time Satellite Data, *GIM*  
495 *INTERNATIONAL*, 18, 41-43, 2004.
- 496 de Foy, B., Wiedinmyer, C., and Schauer, J.: Estimation of mercury emissions from forest fires, lakes, regional and  
497 local sources using measurements in Milwaukee and an inverse method, *Atmospheric Chemistry and Physics*, 12, 8993-  
498 9011, 2012.
- 499 de Foy, B., Lu, Z., and Streets, D. G.: Impacts of control strategies, the great recession and weekday variations on NO<sub>2</sub>  
500 columns above North American cities, *Atmospheric Environment*, 138, 74-86, 2016a.
- 501 de Foy, B., Tong, Y., Yin, X., Zhang, W., Kang, S., Zhang, Q., Zhang, G., Wang, X., and Schauer, J. J.: First field-  
502 based atmospheric observation of the reduction of reactive mercury driven by sunlight, *Atmospheric Environment*, 134, 27-  
503 39, 2016b.
- 504 de Foy, B., Lu, Z., and Streets, D. G.: Satellite NO<sub>2</sub> retrievals suggest China has exceeded its NO<sub>x</sub> reduction goals



- 505 from the twelfth Five-Year Plan, Scientific reports, 6, 35912, 2016c.
- 506 de Foy, B.: City-level variations in NO<sub>x</sub> emissions derived from hourly monitoring data in Chicago, Atmospheric  
507 Environment, 2017.
- 508 Denzler, B., Bogdal, C., Henne, S., Obrist, D., Steinbacher, M., and Hungerbühler, K.: Inversion Approach to Validate  
509 Mercury Emissions Based on Background Air Monitoring at the High Altitude Research Station Jungfrauojoch (3580 m),  
510 Environmental Science & Technology, 51, 2846-2853, 2017.
- 511 Draxler, R. R., and Rolph, G.: HYSPLIT (HYbrid Single-Particle Lagrangian Integrated Trajectory) model access via  
512 NOAA ARL READY website (<http://www.arl.noaa.gov/ready/hysplit4.html>). NOAA Air Resources Laboratory, Silver  
513 Spring, in, Md, 2003.
- 514 Ebinghaus, R., Kock, H., Coggins, A., Spain, T., Jennings, S., and Temme, C.: Long-term measurements of  
515 atmospheric mercury at Mace Head, Irish west coast, between 1995 and 2001, Atmospheric Environment, 36, 5267-5276,  
516 2002.
- 517 Fang, F., Wang, Q., and Li, J.: Urban environmental mercury in Changchun, a metropolitan city in Northeastern China:  
518 source, cycle, and fate, Science of the Total Environment, 330, 159-170, 2004.
- 519 Feng, X., Tang, S., Shang, L., Yan, H., Sommar, J., and Lindqvist, O.: Total gaseous mercury in the atmosphere of  
520 Guiyang, PR China, Science of the Total Environment, 304, 61-72, 2003.
- 521 Feng, X., Shang, L., Wang, S., Tang, S., and Zheng, W.: Temporal variation of total gaseous mercury in the air of  
522 Guiyang, China, Journal of Geophysical Research: Atmospheres, 109, 2004.
- 523 Fu, X., Feng, X., Zhu, W., Wang, S., and Lu, J.: Total gaseous mercury concentrations in ambient air in the eastern  
524 slope of Mt. Gongga, South-Eastern fringe of the Tibetan plateau, China, Atmospheric Environment, 42, 970-979, 2008.
- 525 Fu, X., Feng, X., Wang, S., Rothenberg, S., Shang, L., Li, Z., and Qiu, G.: Temporal and spatial distributions of total  
526 gaseous mercury concentrations in ambient air in a mountainous area in southwestern China: Implications for industrial and  
527 domestic mercury emissions in remote areas in China, Science of the total environment, 407, 2306-2314, 2009.
- 528 Fu, X., Feng, X., Dong, Z., Yin, R., Wang, J., Yang, Z., and Zhang, H.: Atmospheric gaseous elemental mercury  
529 (GEM) concentrations and mercury depositions at a high-altitude mountain peak in south China, Atmospheric Chemistry and  
530 Physics, 10, 2425-2437, 2010.
- 531 Fu, X., Feng, X., Qiu, G., Shang, L., and Zhang, H.: Speciated atmospheric mercury and its potential source in Guiyang,  
532 China, Atmospheric environment, 45, 4205-4212, 2011.
- 533 Fu, X., Feng, X., Liang, P., Zhang, H., Ji, J., and Liu, P.: Temporal trend and sources of speciated atmospheric mercury  
534 at Waliguan GAW station, Northwestern China, Atmospheric Chemistry and Physics, 12, 1951-1964, 2012a.
- 535 Fu, X., Feng, X., Shang, L., Wang, S., and Zhang, H.: Two years of measurements of atmospheric total gaseous  
536 mercury (TGM) at a remote site in Mt. Changbai area, Northeastern China, Atmospheric Chemistry and Physics, 12, 4215-  
537 4226, 2012b.
- 538 Fu, X., Feng, X., Sommar, J., and Wang, S.: A review of studies on atmospheric mercury in China, Science of the Total  
539 Environment, 421, 73-81, 2012c.
- 540 Fu, X., Maruschak, N., Heimbürger, L.-E., Sauvage, B., Gheusi, F., Prestbo, E. M., and Sonke, J. E.: Atmospheric  
541 mercury speciation dynamics at the high-altitude Pic du Midi Observatory, southern France, Atmos. Chem. Phys., 16, 5623-



- 542 5639, 2016a.
- 543 Fu, X., Zhu, W., Zhang, H., Sommar, J., Yu, B., Yang, X., Wang, X., Lin, C.-J., and Feng, X.: Depletion of atmospheric  
544 gaseous elemental mercury by plant uptake at Mt. Changbai, Northeast China, *Atmospheric Chemistry and Physics*, 16,  
545 12861-12873, 2016b.
- 546 Gautam, R., Hsu, N., Tsay, S., Lau, K., Holben, B., Bell, S., Smirnov, A., Li, C., Hansell, R., and Ji, Q.: Accumulation  
547 of aerosols over the Indo-Gangetic plains and southern slopes of the Himalayas: distribution, properties and radiative effects  
548 during the 2009 pre-monsoon season, *Atmospheric Chemistry and Physics*, 11, 12841-12863, 2011.
- 549 Giglio, L., Descloitres, J., Justice, C. O., and Kaufman, Y. J.: An enhanced contextual fire detection algorithm for  
550 MODIS, *Remote sensing of environment*, 87, 273-282, 2003.
- 551 Gratz, L., Esposito, G., Dalla Torre, S., Cofone, F., Pirrone, N., and Sprovieri, F.: First Measurements of Ambient Total  
552 Gaseous Mercury (TGM) at the EvK2CNR Pyramid Observatory in Nepal, *E3S Web of Conferences*, 2013.
- 553 Holmes, C. D., Jacob, D. J., Corbitt, E. S., Mao, J., Yang, X., Talbot, R., and Slemr, F.: Global atmospheric model for  
554 mercury including oxidation by bromine atoms, *Atmospheric Chemistry and Physics*, 10, 12037-12057, 2010.
- 555 Howard, D., and Edwards, G. C.: Mercury fluxes over an Australian alpine grassland and observation of nocturnal  
556 atmospheric mercury depletion events, *Atmos. Chem. Phys. Discuss.*, <https://doi.org/10.5194/acp-2017-580>, in review,  
557 2017.
- 558 Huang, J., Kang, S., Zhang, Q., Yan, H., Guo, J., Jenkins, M. G., Zhang, G., and Wang, K.: Wet deposition of mercury  
559 at a remote site in the Tibetan Plateau: concentrations, speciation, and fluxes, *Atmospheric Environment*, 62, 540-550, 2012.
- 560 Huang, J., Kang, S., Wang, S., Wang, L., Zhang, Q., Guo, J., Wang, K., Zhang, G., and Tripathee, L.: Wet deposition of  
561 mercury at Lhasa, the capital city of Tibet, *Science of the total environment*, 447, 123-132, 2013.
- 562 Kang, S., Huang, J., Wang, F., Zhang, Q., Zhang, Y., Li, C., Wang, L., Chen, P., Sharma, C. M., and Li, Q.:  
563 Atmospheric mercury depositional chronology reconstructed from lake sediments and ice core in the Himalayas and Tibetan  
564 Plateau, *Environmental science & technology*, 50, 2859-2869, 2016.
- 565 Karunasagar, D., Krishna, M. B., Anjaneyulu, Y. a., and Arunachalam, J.: Studies of mercury pollution in a lake due to  
566 a thermometer factory situated in a tourist resort: Kodaikkanal, India, *Environmental pollution*, 143, 153-158, 2006.
- 567 Kellerhals, M., Beauchamp, S., Belzer, W., Blanchard, P., Froude, F., Harvey, B., McDonald, K., Pilote, M., Poissant,  
568 L., and Puckett, K.: Temporal and spatial variability of total gaseous mercury in Canada: results from the Canadian  
569 Atmospheric Mercury Measurement Network (CAMNet), *Atmospheric Environment*, 37, 1003-1011, 2003.
- 570 Kim, S. Y.: Continental outflow of polluted air from the US to the North Atlantic and mercury chemical cycling in  
571 various atmospheric environments, University of New Hampshire (Natural Resources and Earth Systems Science Program),  
572 2010.
- 573 Kocman, D., and Horvat, M.: A laboratory based experimental study of mercury emission from contaminated soils in  
574 the River Idrijca catchment, *Atmospheric Chemistry and Physics*, 10, 1417-1426, 2010.
- 575 Lan, X., Talbot, R., Castro, M., Perry, K., and Luke, W.: Seasonal and diurnal variations of atmospheric mercury across  
576 the US determined from AMNet monitoring data, *Atmospheric Chemistry and Physics*, 12, 10569, 2012.
- 577 Landis, M. S., Stevens, R. K., Schaedlich, F., and Prestbo, E. M.: Development and characterization of an annular  
578 denuder methodology for the measurement of divalent inorganic reactive gaseous mercury in ambient air, *Environmental*



- 579 science & technology, 36, 3000-3009, 2002.
- 580 Li, C., Kang, S., Zhang, Q., and Kaspari, S.: Major ionic composition of precipitation in the Nam Co region, Central  
581 Tibetan Plateau, Atmospheric Research, 85, 351-360, 2007.
- 582 Li, C., Bosch, C., Kang, S., Andersson, A., Chen, P., Zhang, Q., Cong, Z., Chen, B., Qin, D., and Gustafsson, Ö.:  
583 Sources of black carbon to the Himalayan–Tibetan Plateau glaciers, Nature Communications, 7, 12574, 2016.
- 584 Liu, S., Nadim, F., Perkins, C., Carley, R. J., Hoag, G. E., Lin, Y., and Chen, L.: Atmospheric mercury monitoring  
585 survey in Beijing, China, Chemosphere, 48, 97-107, 2002.
- 586 Liu, N., Qiu, G., Landis, M. S., Feng, X., Fu, X., and Shang, L.: Atmospheric mercury species measured in Guiyang,  
587 Guizhou province, southwest China, Atmospheric Research, 100, 93-102, 2011.
- 588 Liu, Y., Wang, Y., Pan, Y., and Piao, S.: Wet deposition of atmospheric inorganic nitrogen at five remote sites in the  
589 Tibetan Plateau, Atmospheric Chemistry and Physics, 15, 11683-11700, 2015.
- 590 Ma, Y., Kang, S., Zhu, L., Xu, B., Tian, L., and Yao, T.: ROOF OF THE WORLD: Tibetan observation and research  
591 platform: atmosphere–land interaction over a heterogeneous landscape, Bulletin of the American Meteorological Society, 89,  
592 1487-1492, 2008.
- 593 Mallik, C., and Lal, S.: Seasonal characteristics of SO<sub>2</sub>, NO<sub>2</sub>, and CO emissions in and around the Indo-Gangetic Plain,  
594 Environmental monitoring and assessment, 186, 1295-1310, 2014.
- 595 Mukherjee, A. B., Bhattacharya, P., Sarkar, A., and Zevenhoven, R.: Mercury emissions from industrial sources in India  
596 and its effects in the environment, in: Mercury Fate and Transport in the Global Atmosphere, Springer, 81-112, 2009.
- 597 Obrist, D., Tas, E., Peleg, M., Matveev, V., Faïn, X., Asaf, D., and Luria, M.: Bromine-induced oxidation of mercury in  
598 the mid-latitude atmosphere, Nature Geoscience, 4, 22-26, 2011.
- 599 Pacyna, E. G., Pacyna, J., Sundseth, K., Munthe, J., Kindbom, K., Wilson, S., Steenhuisen, F., and Maxson, P.: Global  
600 emission of mercury to the atmosphere from anthropogenic sources in 2005 and projections to 2020, Atmospheric  
601 Environment, 44, 2487-2499, 2010.
- 602 Park, S.-Y., Holsen, T. M., Kim, P.-R., and Han, Y.-J.: Laboratory investigation of factors affecting mercury emissions  
603 from soils, Environmental earth sciences, 72, 2711-2721, 2014.
- 604 Parvathi, K., Jayaprakash, K., and Sivakumar, N.: Mercury contamination due to thermometer glass solid waste  
605 dumping-a preliminary report, Asian Journal of Experimental Chemistry, 5, 46-48, 2010.
- 606 Peng, G., Qinghua, Y., and Qiufang, W.: Lake ice change at the Nam Co Lake on the Tibetan Plateau during 2000-2013  
607 and influencing factors, PROGRESS IN GEOGRAPHY, 34, 1241-1249.
- 608 Peterson, C., Gustin, M., and Lyman, S.: Atmospheric mercury concentrations and speciation measured from 2004 to  
609 2007 in Reno, Nevada, USA, Atmospheric Environment, 43, 4646-4654, 2009.
- 610 Pirrone, N., Cinnirella, S., Feng, X., Finkelman, R., Friedli, H., Leaner, J., Mason, R., Mukherjee, A., Stracher, G., and  
611 Streets, D.: Global mercury emissions to the atmosphere from anthropogenic and natural sources, Atmospheric Chemistry  
612 and Physics, 10, 5951-5964, 2010.
- 613 Poissant, L., Pilote, M., Beauvais, C., Constant, P., and Zhang, H. H.: A year of continuous measurements of three  
614 atmospheric mercury species (GEM, RGM and Hg p) in southern Quebec, Canada, Atmospheric Environment, 39, 1275-  
615 1287, 2005.



- 616 Polissar, A., Hopke, P., Paatero, P., Kaufmann, Y., Hall, D., Bodhaine, B., Dutton, E., and Harris, J.: The aerosol at  
617 Barrow, Alaska: long-term trends and source locations, *Atmospheric Environment*, 33, 2441-2458, 1999.
- 618 Rao, S., Zurbenko, I., Neagu, R., Porter, P., Ku, J., and Henry, R.: Space and time scales in ambient ozone data,  
619 *Bulletin of the American Meteorological Society*, 78, 2153-2166, 1997.
- 620 Schroeder, W. H., and Munthe, J.: Atmospheric mercury—an overview, *Atmospheric Environment*, 32, 809-822, 1998.
- 621 Selin, H.: Global environmental law and treaty-making on hazardous substances: the Minamata Convention and  
622 mercury abatement, *Global Environmental Politics*, 14, 1-19, 2014.
- 623 Sheng, J., Wang, X., Gong, P., Joswiak, D. R., Tian, L., Yao, T., and Jones, K. C.: Monsoon-driven transport of  
624 organochlorine pesticides and polychlorinated biphenyls to the Tibetan Plateau: three year atmospheric monitoring study,  
625 *Environmental science & technology*, 47, 3199-3208, 2013.
- 626 Sheu, G.-R., Lin, N.-H., Wang, J.-L., Lee, C.-T., Yang, C.-F. O., and Wang, S.-H.: Temporal distribution and potential  
627 sources of atmospheric mercury measured at a high-elevation background station in Taiwan, *Atmospheric Environment*, 44,  
628 2393-2400, 2010.
- 629 Shia, R. L., Seigneur, C., Pai, P., Ko, M., and Sze, N. D.: Global simulation of atmospheric mercury concentrations and  
630 deposition fluxes, *Journal of Geophysical Research: Atmospheres*, 104, 23747-23760, 1999.
- 631 Shichang, K., Yongping, Y., and Liping, Z.: *Modern Environmental Process and Changes in the Basin of Nam Co in*  
632 *Tibetan Plateau*, in: Beijing: China Meteorological Press (in Chinese with English abstract), 2011.
- 633 Sigler, J., Mao, H., and Talbot, R.: Gaseous elemental and reactive mercury in Southern New Hampshire, *Atmospheric*  
634 *Chemistry and Physics*, 9, 1929-1942, 2009.
- 635 Slemr, F., Brunke, E.-G., Ebinghaus, R., and Kuss, J.: Worldwide trend of atmospheric mercury since 1995,  
636 *Atmospheric Chemistry and Physics*, 11, 4779-4787, 2011.
- 637 Sprovieri, F., Pirrone, N., Bencardino, M., D'Amore, F., Carbone, F., Cinnirella, S., Mannarino, V., Landis, M.,  
638 Ebinghaus, R., and Weigelt, A.: Atmospheric mercury concentrations observed at ground-based monitoring sites globally  
639 distributed in the framework of the GMOS network, *Atmospheric Chemistry and Physics*, 16, 11915-11935, 2016.
- 640 Streets, D. G., Hao, J., Wu, Y., Jiang, J., Chan, M., Tian, H., and Feng, X.: Anthropogenic mercury emissions in China,  
641 *Atmospheric Environment*, 39, 7789-7806, 2005.
- 642 Su, J., Cheng, J.-p., Ye, X., Yuan, T., Wang, W., and Mi, L.: Preliminary study on mercury distribution in multimedia  
643 environment in Lanzhou, *Journal of Agro-Environment Science*, 26, 381-385, 2007.
- 644 Subramanian, V.: Water quality in south Asia, *Asian journal of water, Environment and Pollution*, 1, 41-54, 2004.
- 645 Tong, Y., Yin, X., Lin, H., Wang, H., Deng, C., Chen, L., Li, J., Zhang, W., Schauer, J. J., and Kang, S.: Recent  
646 Decline of Atmospheric Mercury Recorded by *Androsace tapete* on the Tibetan Plateau, *Environmental Science &*  
647 *Technology*, 50, 13224-13231, 2016.
- 648 Wan, Q., Feng, X., Lu, J., Zheng, W., Song, X., Han, S., and Xu, H.: Atmospheric mercury in Changbai Mountain area,  
649 northeastern China I. The seasonal distribution pattern of total gaseous mercury and its potential sources, *Environmental*  
650 *research*, 109, 201-206, 2009.
- 651 Wan, X., Kang, S., Wang, Y., Xin, J., Liu, B., Guo, Y., Wen, T., Zhang, G., and Cong, Z.: Size distribution of  
652 carbonaceous aerosols at a high-altitude site on the central Tibetan Plateau (Nam Co Station, 4730 m asl), *Atmospheric*





- 653 Research, 153, 155-164, 2015.
- 654 Wang, B., and Fan, Z.: Choice of South Asian summer monsoon indices, *Bulletin of the American Meteorological*  
655 *Society*, 80, 629-638, 1999.
- 656 Wang, B., Wu, R., and Lau, K.: Interannual variability of the Asian summer monsoon: Contrasts between the Indian  
657 and the western North Pacific–East Asian monsoons, *Journal of climate*, 14, 4073-4090, 2001.
- 658 Wang, Y., Zhang, X., and Draxler, R. R.: TrajStat: GIS-based software that uses various trajectory statistical analysis  
659 methods to identify potential sources from long-term air pollution measurement data, *Environmental Modelling & Software*,  
660 24, 938-939, 2009.
- 661 Wang, Y.: MeteoInfo: GIS software for meteorological data visualization and analysis, *Meteorological Applications*,  
662 21, 360-368, 2014.
- 663 Wang, Y., Zhang, Y., Schauer, J. J., de Foy, B., Guo, B., and Zhang, Y.: Relative impact of emissions controls and  
664 meteorology on air pollution mitigation associated with the Asia-Pacific Economic Cooperation (APEC) conference in  
665 Beijing, China, *Science of The Total Environment*, 571, 1467-1476, 2016.
- 666 Wang, Y., de Foy, B., Schauer, J. J., Olson, M. R., Zhang, Y., Li, Z., and Zhang, Y.: Impacts of regional transport on  
667 black carbon in Huairou, Beijing, China, *Environmental Pollution*, 221, 75-84, 2017.
- 668 Weiss-Penzias, P., Jaffe, D. A., McClintick, A., Prestbo, E. M., and Landis, M. S.: Gaseous elemental mercury in the  
669 marine boundary layer: Evidence for rapid removal in anthropogenic pollution, *Environmental science & technology*, 37,  
670 3755-3763, 2003.
- 671 Wu, Q., Wang, S., Li, G., Liang, S., Lin, C.-J., Wang, Y., Cai, S., Liu, K., and Hao, J.: Temporal Trend and Spatial  
672 Distribution of Speciated Atmospheric Mercury Emissions in China During 1978–2014, *Environmental Science &*  
673 *Technology*, 50, 13428-13435, 2016.
- 674 Wu, Q., Gao, W., Wang, S., and Hao, J.: Updated atmospheric speciated mercury emissions from iron and steel  
675 production in China during 2000–2015, *Atmospheric Chemistry and Physics*, 17, 10423-10433, 2017.
- 676 Xia, X., Zong, X., Cong, Z., Chen, H., Kang, S., and Wang, P.: Baseline continental aerosol over the central Tibetan  
677 plateau and a case study of aerosol transport from South Asia, *Atmospheric environment*, 45, 7370-7378, 2011.
- 678 Xiang, J., and Liu, G.: Distribution and sources of atmospheric mercury in urban areas of Wuhan, *Resour. Environ.*  
679 *Eng.*, 22, 27-30, 2008.
- 680 Xiao, H., Shen, L., Su, Y., Barresi, E., DeJong, M., Hung, H., Lei, Y.-D., Wania, F., Reiner, E. J., and Sverko, E.:  
681 Atmospheric concentrations of halogenated flame retardants at two remote locations: The Canadian High Arctic and the  
682 Tibetan Plateau, *Environmental pollution*, 161, 154-161, 2012.
- 683 Xiu, G., Cai, J., Zhang, W., Zhang, D., Büeler, A., Lee, S., Shen, Y., Xu, L., Huang, X., and Zhang, P.: Speciated  
684 mercury in size-fractionated particles in Shanghai ambient air, *Atmospheric Environment*, 43, 3145-3154, 2009.
- 685 Xu, L., Chen, J., Yang, L., Niu, Z., Tong, L., Yin, L., and Chen, Y.: Characteristics and sources of atmospheric mercury  
686 speciation in a coastal city, Xiamen, China, *Chemosphere*, 119, 530-539, 2015.
- 687 Yang, H., Battarbee, R. W., Turner, S. D., Rose, N. L., Derwent, R. G., Wu, G., and Yang, R.: Historical reconstruction  
688 of mercury pollution across the Tibetan Plateau using lake sediments, *Environmental science & technology*, 44, 2918-2924,  
689 2010.



- 690 Yao, T., Thompson, L., Yang, W., Yu, W., Gao, Y., Guo, X., Yang, X., Duan, K., Zhao, H., and Xu, B.: Different  
691 glacier status with atmospheric circulations in Tibetan Plateau and surroundings, *Nature climate change*, 2, 663-667, 2012.
- 692 Yaqiong, L., Yaoming, M., and Maoshan, L.: Study on characteristic of atmospheric boundary layer over Lake Namco  
693 region, Tibetan Plateau, *Plateau Meteorology (in Chinese)*, 27, 1205-1210, 2008.
- 694 Yatawelli, R. L., Fahrni, J. K., Kim, M., Crist, K. C., Vickers, C. D., Winter, S. E., and Connell, D. P.: Mercury, PM 2.5  
695 and gaseous co-pollutants in the Ohio River Valley region: Preliminary results from the Athens supersite, *Atmospheric  
696 environment*, 40, 6650-6665, 2006.
- 697 Yin, X., Kang, S., de Foy, B., Cong, Z., Luo, J., Lang, Z., Ma, Y., Zhang, G., Rupakheti, D., and Zhang, Q.: Surface  
698 ozone at Nam Co in the inland Tibetan Plateau: variation, synthesis comparison and regional representativeness,  
699 *Atmospheric Chemistry and Physics*, 17, 11293-11311, 2017.
- 700 You, Q., Kang, S., Li, C., Li, M., and Liu, J.: Variation features of meteorological elements at Namco Station, Tibetan  
701 Plateau, *Meteorological Monthly*, 33, 54-60, 2007.
- 702 Zhang, L., Wang, S., Wang, L., and Hao, J.: Atmospheric mercury concentration and chemical speciation at a rural site  
703 in Beijing, China: implications of mercury emission sources, *Atmospheric Chemistry and Physics*, 13, 10505-10516, 2013.
- 704 Zhang, Q., Pan, K., Kang, S., Zhu, A., and Wang, W.-X.: Mercury in wild fish from high-altitude aquatic ecosystems in  
705 the Tibetan Plateau, *Environmental science & technology*, 48, 5220-5228, 2014.
- 706 Zhang, H., Fu, X., Lin, C., Wang, X., and Feng, X.: Observation and analysis of speciated atmospheric mercury in  
707 Shangri-La, Tibetan Plateau, China, *Atmos. Chem. Phys.*, 15, 653-665, 2015.
- 708 Zhang, X., Ming, J., Li, Z., Wang, F., and Zhang, G.: The online measured black carbon aerosol and source orientations  
709 in the Nam Co region, Tibet, *Environmental Science and Pollution Research*, 24, 25021-25033, 2017.
- 710 Zhang, Y., Jacob, D. J., Horowitz, H. M., Chen, L., Amos, H. M., Krabbenhoft, D. P., Slemr, F., Louis, V. L. S., and  
711 Sunderland, E. M.: Observed decrease in atmospheric mercury explained by global decline in anthropogenic emissions,  
712 *Proceedings of the National Academy of Sciences*, 113, 526-531, 2016.
- 713 Zhu, J., Wang, T., Talbot, R., Mao, H., Hall, C., Yang, X., Fu, C., Zhuang, B., Li, S., and Han, Y.: Characteristics of  
714 atmospheric total gaseous mercury (TGM) observed in urban Nanjing, China, *Atmospheric Chemistry and Physics*, 12,  
715 12103-12118, 2012.
- 716  
717  
718  
719  
720  
721  
722  
723  
724  
725  
726



727

728

729

**Table 1. The statistics of TGM and meteorological variables in different seasons at the Nam Co Station during the measurement period (2012-2014).**

Period	Statistical	TGM (ng m <sup>-3</sup> )	T (°C)	RH (%)	WS (m s <sup>-1</sup> )
Total	Mean	1.33	-0.29	50.67	3.32
	Median	1.34	0.30	50.00	2.80
	Standard Deviation	0.24	8.98	22.37	2.22
	Minimum	0.23	-28.90	5.30	0.00
	Maximum	3.14	19.00	98.00	15.60
	Count	14408	20695	20695	20695
Spring (MAM)	Mean	1.28	-0.90	51.58	3.21
	Median	1.30	-0.60	50.30	2.80
	Standard Deviation	0.20	6.48	24.38	2.11
	Minimum	0.42	-21.20	5.30	0.00
	Maximum	2.41	17.90	98.00	12.80
	Count	4506	4980	4980	4980
Summer (JJA)	Mean	1.50	8.80	63.32	2.94
	Median	1.50	8.60	65.30	2.60
	Standard Deviation	0.20	3.59	18.25	1.74
	Minimum	0.23	-4.10	11.00	0.00
	Maximum	3.14	19.00	97.00	11.10
	Count	5243	5805	5805	5805
Autumn (SON)	Mean	1.22	-0.78	47.06	3.36
	Median	1.20	-0.40	46.00	2.90
	Standard Deviation	0.17	7.23	20.55	2.07
	Minimum	0.87	-24.80	8.00	0.00
	Maximum	2.68	14.60	97.00	12.90
	Count	2267	4800	4800	4800
Winter (DJF)	Mean	1.14	-9.57	38.81	3.83
	Median	1.13	-9.00	36.00	3.00
	Standard Deviation	0.18	6.40	18.36	2.78
	Minimum	0.45	-28.90	7.00	0.00
	Maximum	2.08	5.20	91.70	15.60
	Count	2392	5110	5110	5110

730

731

732



733

734

Table 2. Statistics of free parameters in the box model of TGM at the Nam Co Station by season.

	Initial TGM (ng m <sup>-3</sup> )	Morning TGM (7-9) burst (ng m <sup>-2</sup> h <sup>-1</sup> )	Evening TGM (18-22) burst (ng m <sup>-2</sup> h <sup>-1</sup> )	Constant TGM deposition (ng m <sup>-2</sup> h <sup>-1</sup> )	Free tropospheric TGM (ng m <sup>-3</sup> )	TGM lifetime during daylight (day)	root-mean- square error (RMSE)	R <sup>2</sup>
Spring	1.288	58.29	37.66	-1.658	1.228	3.183	0.00983	0.96
Summer	1.521	14.2	25.65	-1.775	1.553	5.991	0.00796	0.91
Autumn	1.211	53.34	9.144	-1.061	1.036	Inf	0.0086	0.93
Winter	1.115	52.92	2.468	0	1.168	2.984	0.00368	0.99

735

736

737

738

739

740

741

742

743

744

745

746

747

748

749

750

751

752

753

754

755

756

757



758

759

760

761

**Table 3. Contribution from the different groups to the total variance of the model. The standard deviation of each group gives a sense of the contribution of each group to the variance in units of  $\text{ng m}^{-3}$ . The variance contribution shows the percentage that each group contributes to the total variance of the model.**

Group name	No. Variables	Std ( $\text{ng m}^{-3}$ )	Variance Contribution (%)
Seasonal Signal	6	0.161	83.70
Diurnal Signal	24	0.036	4.08
WRF PBLH	5	0.034	3.81
Surface O <sub>3</sub> Conc	1	0.032	3.20
Strat. O <sub>3</sub> Tracer	1	0.031	3.04
Local Winds	20	0.020	1.34
Annual Signal	43	0.016	0.86

762

763

764

765

766

767

768

769

770

771

772

773

774

775

776

777

778

779

780

781

782

783

784

785

786



787

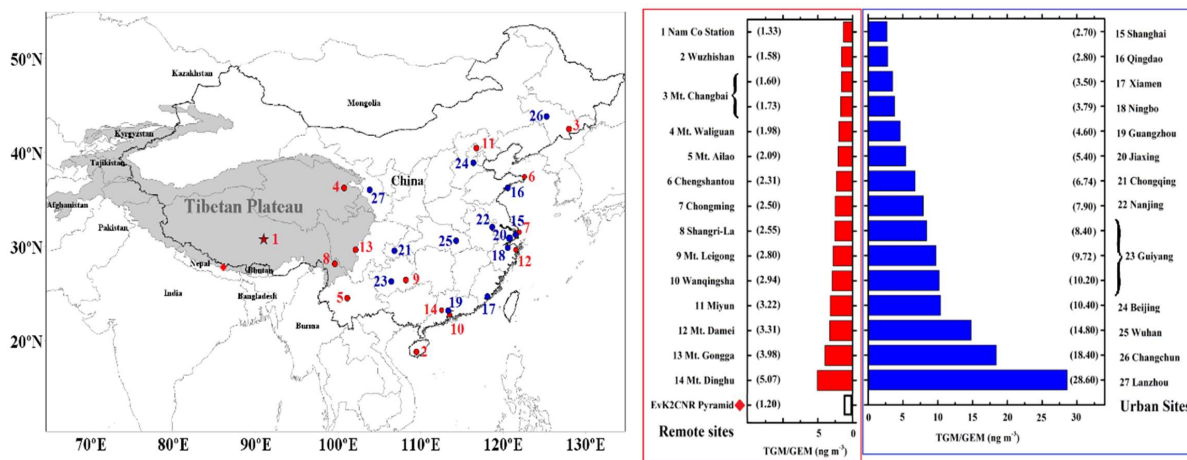
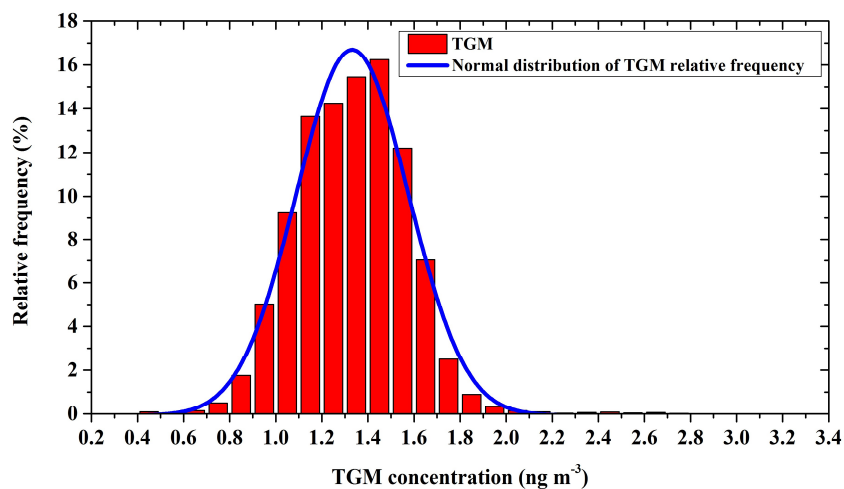


Fig. 1. Geographical location of the Nam Co Station and selected sites with mercury measurements in China.

788  
 789  
 790  
 791  
 792  
 793  
 794  
 795  
 796  
 797  
 798  
 799  
 800  
 801  
 802  
 803  
 804  
 805  
 806  
 807  
 808  
 809



810



811

812

813

814

815

816

817

818

819

820

821

822

823

824

825

826

827

828

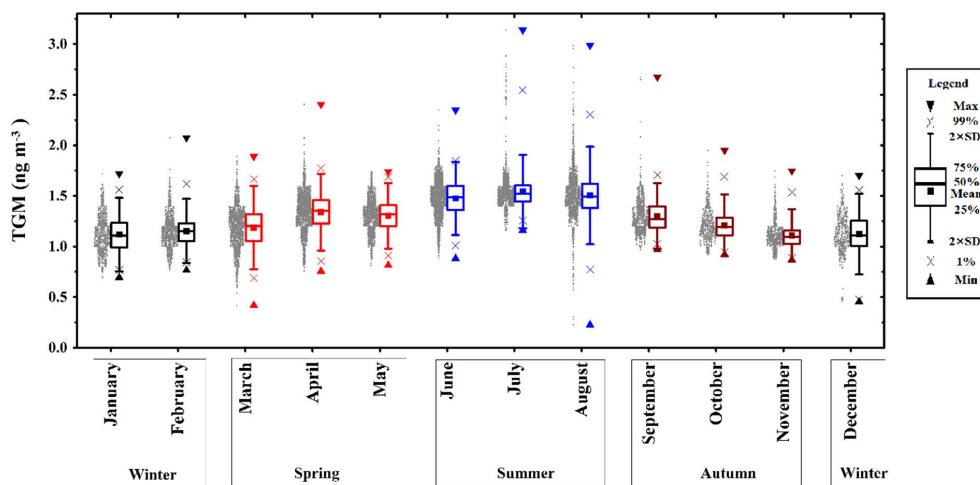
829

830

Fig. 2. Relative frequency plot of TGM distribution data measured at the Nam Co Station.



831



832

833

Fig. 3. Monthly average and statistical parameters of TGM at the Nam Co Station during the whole measurement period (spring (MAM) in red; summer (JJA) in blue; autumn (SON) in dark red; winter (DJF) in black).

834

835

836

837

838

839

840

841

842

843

844

845

846

847

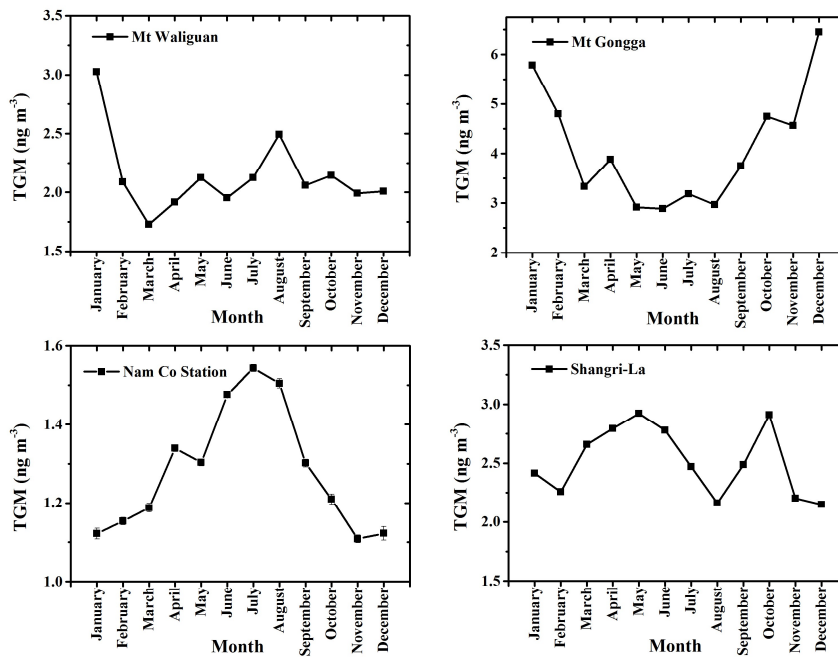
848

849





850



851

852

853 **Fig. 4. Variations of monthly mean TGM at four sites (Mt. Waliguan (Fu et al., 2012a), Nam Co, Mt. Gongga (Fu et al., 2008) and**

854 **Shangri-La (Zhang et al., 2015) in the Tibetan Plateau.**

855

856

857

858

859

860

861

862

863

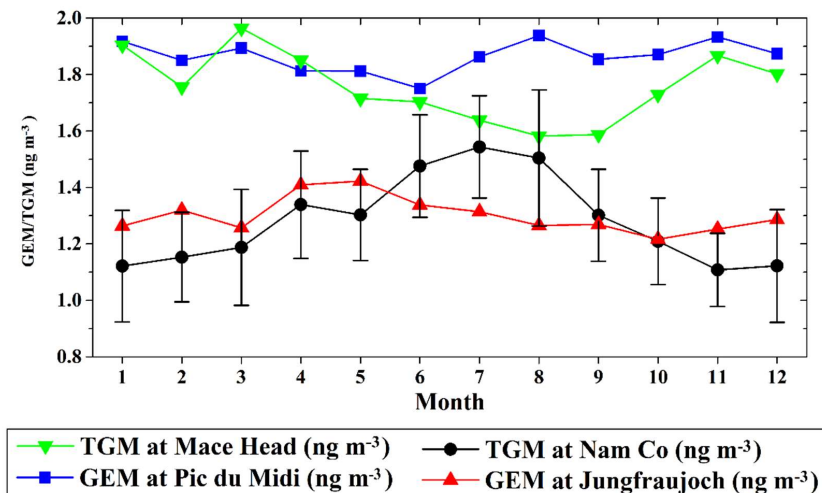
864

865

866



867



868

869

Fig. 5. Monthly average GEM/TGM at three high altitude background stations in the Northern Hemisphere (Denzler et al., 2017;

870

Fu et al., 2016a; Ebinghaus et al., 2002) (average TGM at Mace Head in green; average GEM at Pic du Midi in blue; median GEM

871

at Jungfraujoch in red; average TGM at the Nam Co in black, black bars represent standard deviation at Nam Co).

872

873

874

875

876

877

878

879

880

881

882

883

884

885

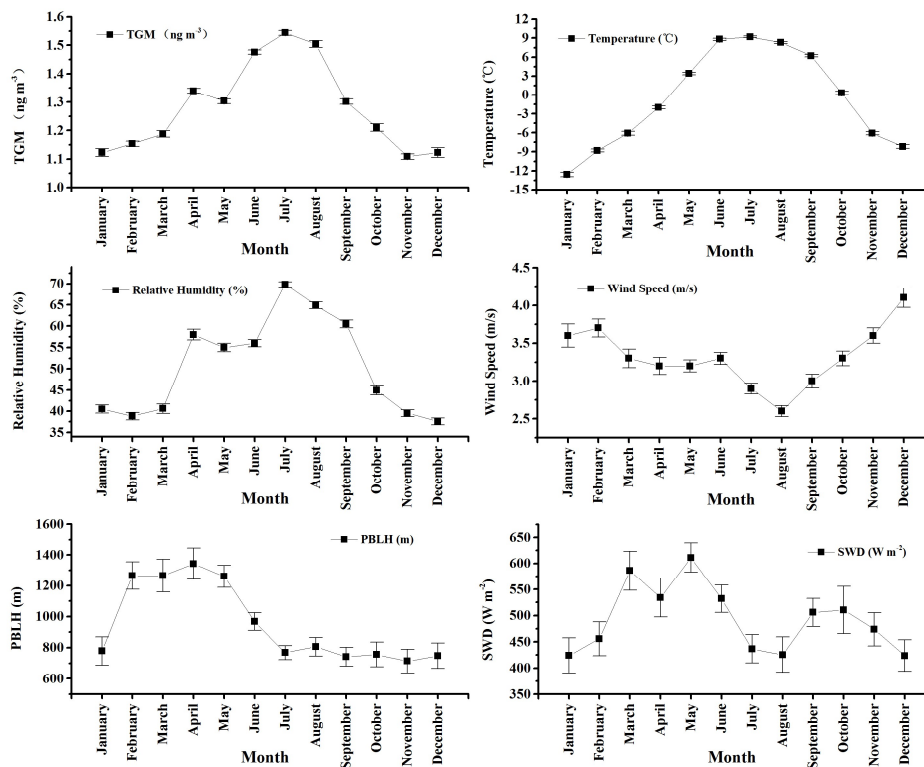
886

887

888



889



890

891

892

**Fig. 6. Monthly variations of TGM, relative humidity, temperature, SWD (downward shortwave radiation), wind speed and PBLH (planetary boundary layer height) during the whole measurement period at the Nam Co Station. Error bars are 95% confidence levels.**

894

895

896

897

898

899

900

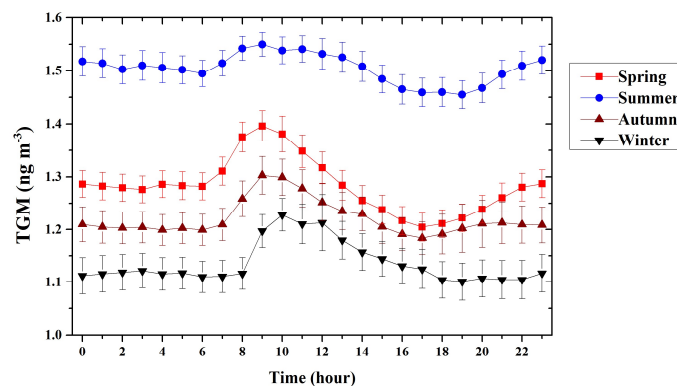
901

902

903



904



905

906 **Fig. 7. Diurnal profiles of average hourly TGM at the Nam Co Station by seasons during the measurement period. Error bars are**

907

95% confidence levels.

908

909

910

911

912

913

914

915

916

917

918

919

920

921

922

923

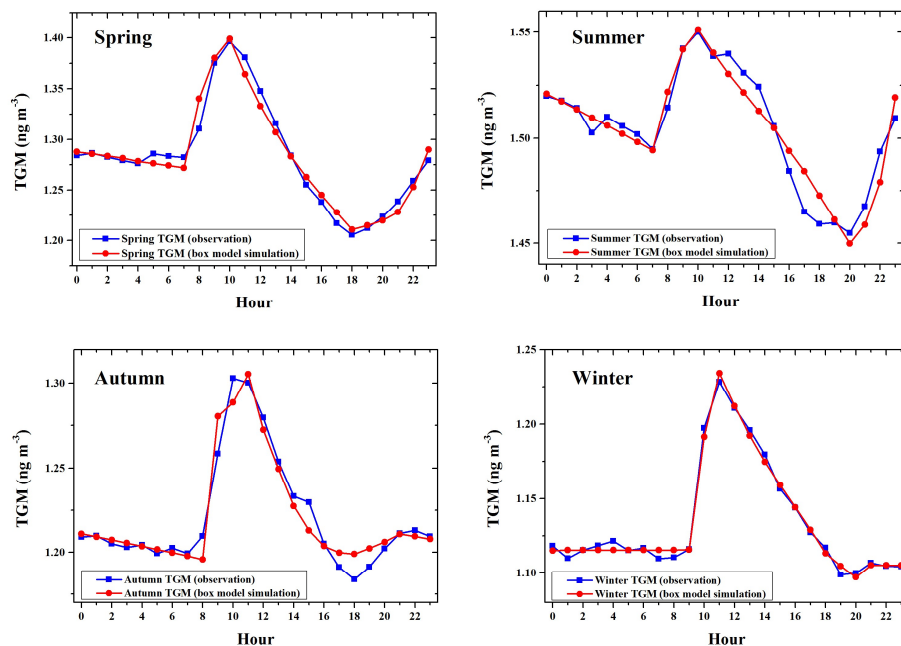
924

925

926



927



928

929

Fig. 8. Diurnal profiles of average hourly TGM at the Nam Co Station by seasons during the measurement period compared with box model simulation.

930

931

932

933

934

935

936

937

938

939

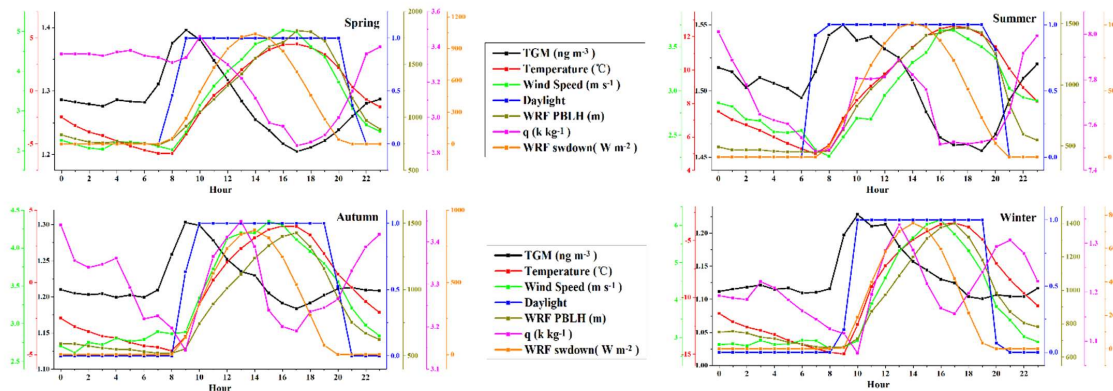
940

941

942



943



944

945

**Fig. 9** Diurnal profiles of TGM and meteorological parameters at the Nam Co Station by season for the measurement period.

946

947

948

949

950

951

952

953

954

955

956

957

958

959

960

961

962

963

964

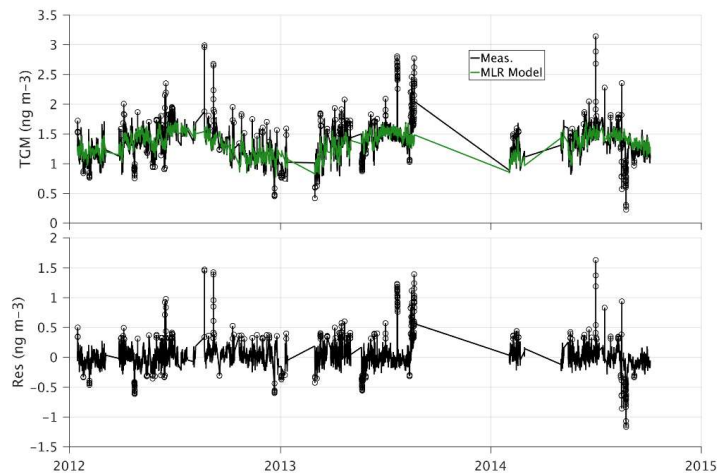
965

966

967



968



969

970

971

**Fig. 10.** The measurements and Multi Linear Regression (MLR) model of TGM (top) and model residual (bottom) (residual = measurement – simulation). The outliers are shown as circles.

972

973

974

975

976

977

978

979

980

981

982

983

984

985

986

987

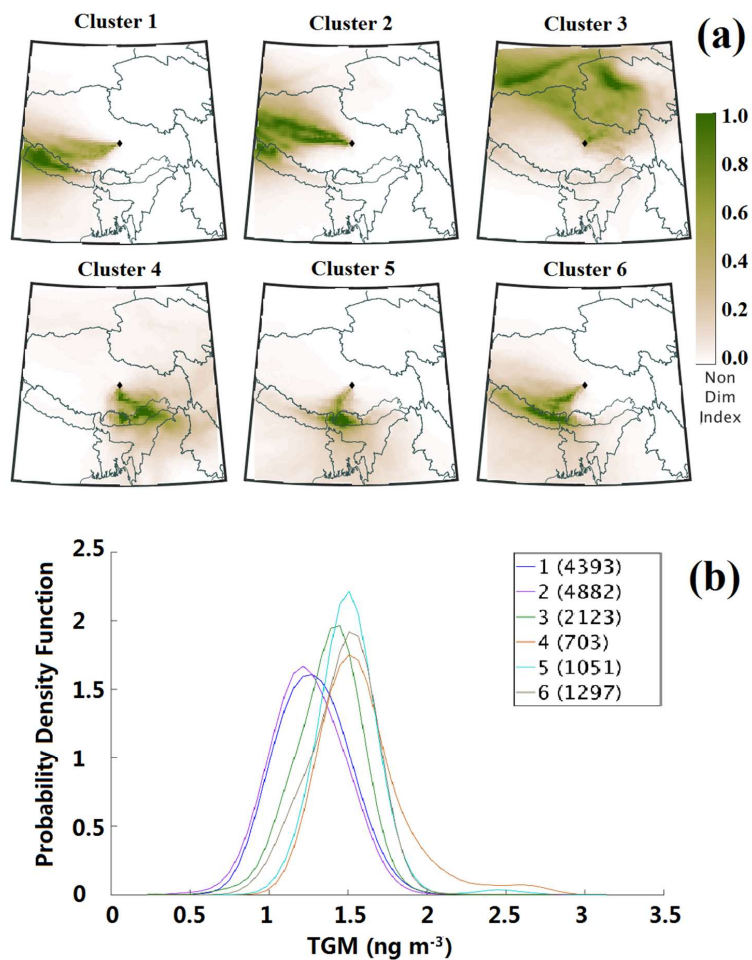
988

989

990



991



992

993

Fig. 11. Clusters of air mass transport to Nam Co using WRF-FLEXPART back-trajectories (a) and probability density function of

994

TGM concentrations for each cluster, with number of data points in parentheses (b).

995

996

997





998

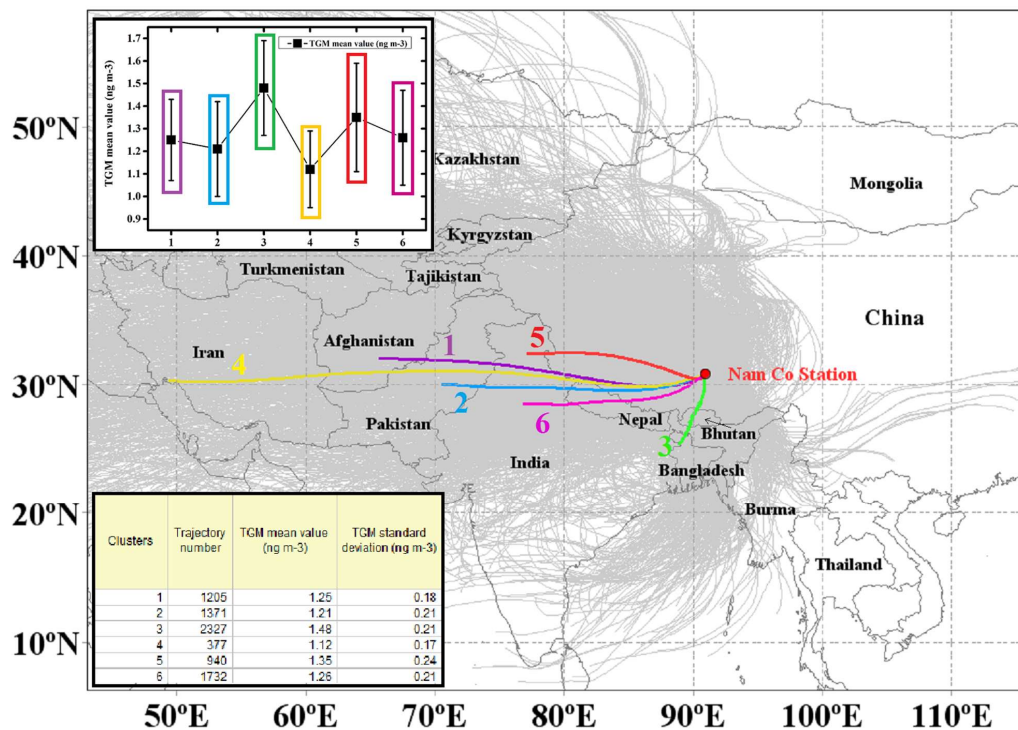
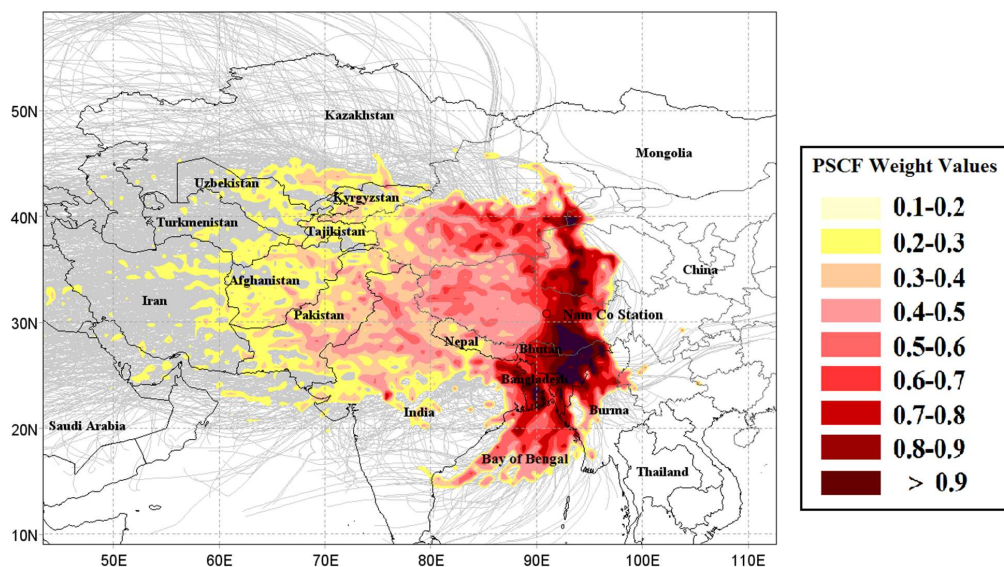


Fig. 12. HYSPLIT backward trajectories (light-gray lines), clusters (color lines) and statistics of clusters (sub-figure and table) during the whole measurement period at the Nam Co Station.

999  
 1000  
 1001  
 1002  
 1003  
 1004  
 1005  
 1006  
 1007  
 1008  
 1009  
 1010  
 1011  
 1012



1013



1014

1015

Fig. 13. Potential Source Contribution Function showing areas with possible emissions or air mass transport associated with higher TGM concentrations at the Nam Co Station during the whole measurement period.

1016

1017

1018

1019

1020

1021

1022

1023

1024

1025

1026

1027

1028

1029

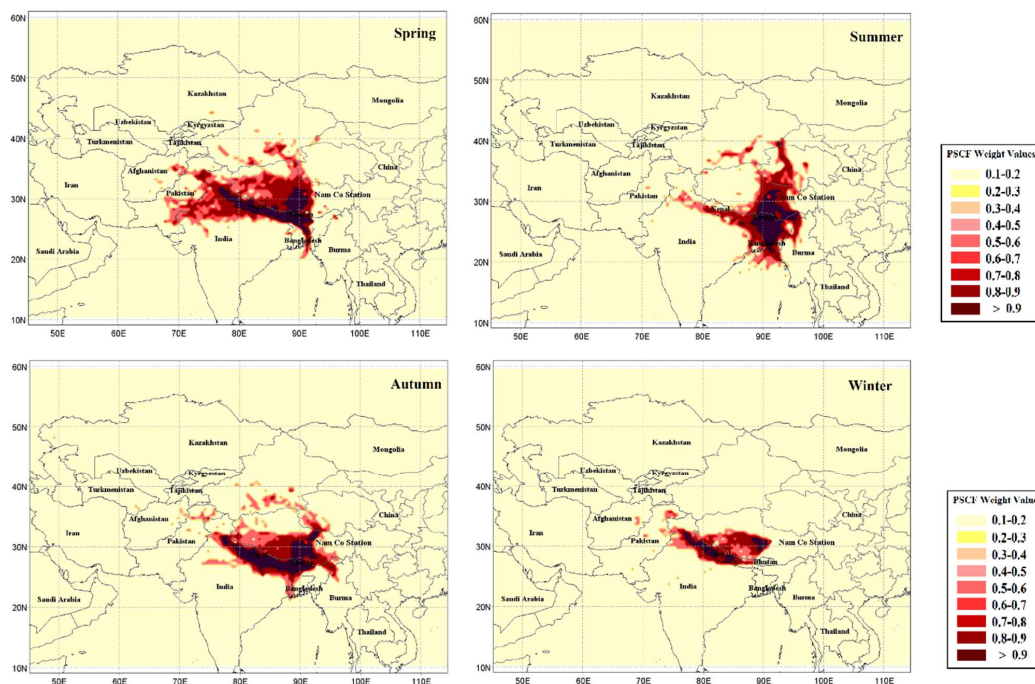
1030

1031

1032



1033



1034

1035

**Fig. 14. Potential Source Contribution Function showing areas with possible emissions or air mass transport associated with higher TGM concentrations at the Nam Co Station by season in 2012.**

1036

1037

1038

1039

1040

1041

1042

1043

1044

1045

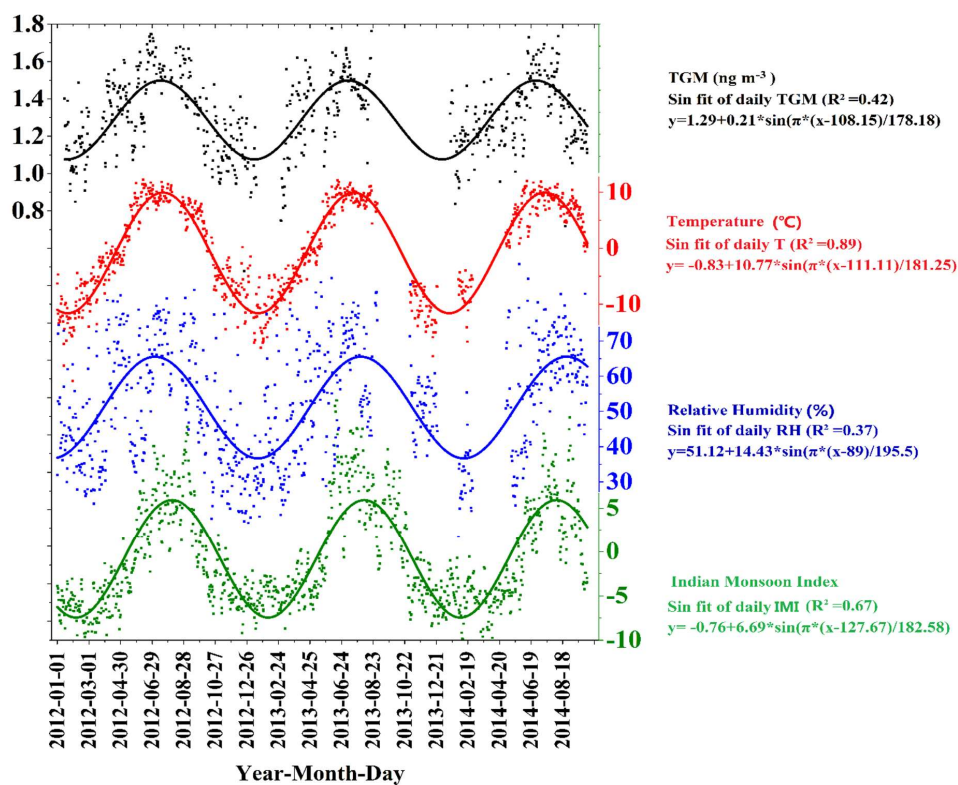
1046

1047

1048



1049



1050

1051

1052 Fig. 15. Series of daily mean TGM, temperature, relative humidity and Indian Monsoon Index and their sinusoidal curve fits.

1053

1054